arXiv:cond-mat/0301325v1 [cond-mat.soft] 17 Jan 2003

Bicontinuous surfaces in self-assembling amphiphilic systems

U. S. Schwarz[1] and G. Gompper[2]

[1]Max-Planck-Institut für Kolloid- und Grenzflächenforschung, D-14424 Potsdam

[2]Institut für Festkörperforschung, Forschungszentrum Jülich, D-52425 Jülich

Appeared in *Morphology of Condensed Matter: Physics and Geometry of Spatially Complex Systems*, eds. K. R. Mecke and D. Stoyan, Springer Lecture Notes in Physics vol. **600**, pp. 107-151 (2002)

Abstract

Amphiphiles are molecules which have both hydrophilic and hydrophobic parts. In water- and/or oil-like solvent, they self-assemble into extended sheet-like structures due to the hydrophobic effect. The free energy of an amphiphilic system can be written as a functional of its interfacial geometry, and phase diagrams can be calculated by comparing the free energies following from different geometries. Here we focus on bicontinuous structures, where one highly convoluted interface spans the whole sample and thereby divides it into two separate labyrinths. The main models for surfaces of this class are triply periodic minimal surfaces, their constant mean curvature and parallel surface companions, and random surfaces. We discuss the geometrical properties of each of these types of surfaces and how they translate into the experimentally observed phase behavior of amphiphilic systems.

1 Surfaces in self-assembling amphiphilic systems

The subject of this article is the theoretical description of amphiphilic systems, which are one example of *soft condensed matter*. Soft matter is material that has a typical energy scale of $k_BT \approx 4 \times 10^{-21}J$, where k_B is the Boltzmann constant and $T \approx 300K$ is room temperature. For such material, perturbations arising from the thermally activated movement of its molecular components are sufficient to induce configurational changes, and entropy is at least equally important as energy in determining its material properties. The understanding of the underlying mechanisms is essential for the application of many technologies in everyday life, including colloidal dispersions (paints, inks, food, creams,

lotions), foams (beverages), liquid crystals (displays), polyelectrolyte gels (diapers) and soaps (washing and cleaning). Moreover, the term *soft matter* also includes most biomaterials, for example blood or cartilage. One particularly important biomaterial is the *biomembrane*, that is the protein carrying lipid bilayer which surrounds each cell and its organelles. A good model system for the structural properties of biomembranes are *lipid bilayers*, which form spontaneously in mixtures of water and lipids and which are one of the main subjects of this paper.

Soft matter systems are very often characterized by competing interactions (including entropic ones), which lead to structure formation on the length scale between tens and hundreds of nanometers (1 nm = 10^{-9} m). Since this length scale is not accessible by optical lithography, self-assembly in soft matter systems is one of the main concepts of nanoscience. With structure formation being so prominent in soft matter systems, their theoretical description often centers around their spatial structure in three dimensions. For a rough classification of the different approaches used, it is convenient to use an analogy to the field of random geometries, and to distinguish between point, fiber and surface processes. Examples of systems which are suited for approaches along these lines are colloidal dispersions, polymer networks and sheet-like structures in self-assembling amphiphilic systems, respectively. Here we will treat the latter case, but we will also show that surface dominated system can be related to Gibbs distributions for scalar fields, namely through the use of isosurface constructions.

Amphiphilic systems are solutions of amphiphiles in suitable solvent. *Amphiphiles* are molecules which consist of two parts, one being hydrophilic (water-like, called the head) and one being hydrophobic (oil-like, called the tail). Well known classes of amphiphiles are *tensides* (used for washing and cleaning purposes) and *lipids* (the basic components of biomembranes). Fig. 1 shows several examples for which phase diagrams are discussed below. Tensides are often called *surfactants*, due to their surface activity at interfaces between water-like and oil-like phases. Hydrophilic and hydrophobic molecules demix due to the hydrophobic effect: oil-like molecules are expelled from a region of water-like molecules since they disturb their network of hydrogen bonds. Hydrophilic and hydrophobic parts of an amphiphilic molecule cannot demix due to the covalent linkage between them, but the amphiphiles can self-assemble in such a way as to shield its hydrophilic parts from its hydrophobic ones and vice versa. Amphiphilic systems have many similarities with diblock copolymer systems, for which the term *microphase separation* is used to denote the molecular tendency for structure formation (see the contribution by Robert Magerle). However, in contrast to diblock copolymers, amphiphiles are small molecules, thus the entropy of their molecular configurations plays only a minor role in determining the overall structure. Moreover, whereas in diblock copolymer systems one component is sufficient to obtain stable mesophases, in amphiphilic systems usually the presence of an aqueous solvent is necessary to obtain well-pronounced structure formation. Both diblock copolymer and amphiphilic systems show structure formation on the nanometer scale, but the length scale is set by dif-

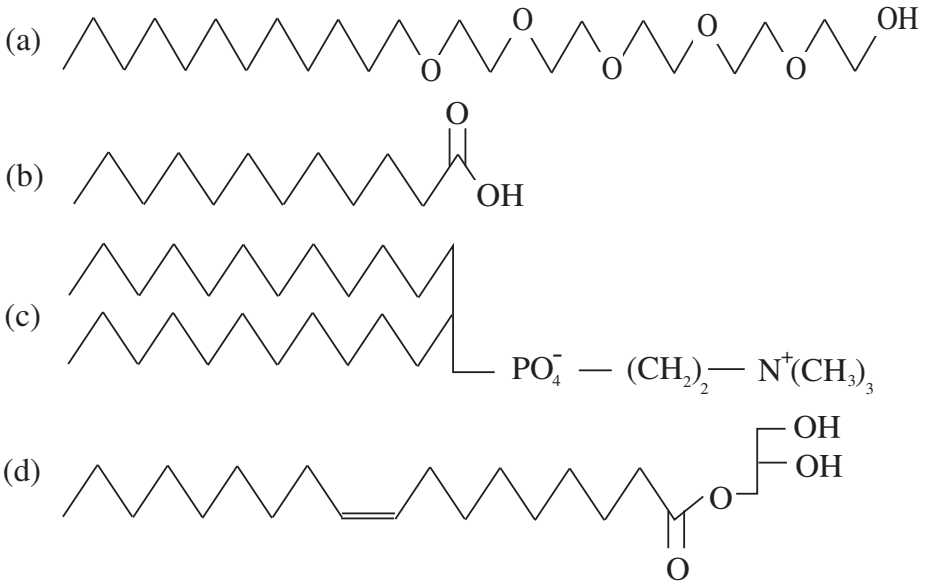

Figure 1: Schematic representation of different amphiphilic molecules. Hydrophobic tails are to the left, hydrophilic heads to the right. (a) Pentaethylene glycol dodecyl ether, $C_{12}H_{25}(OCH_2CH_2)_5OH$ or in short $C_{12}E_5$, is a small surfactant. (b) Lauric acid, $CH_3(CH_2)_{10}COOH$ or in short LA. Fatty acids are the simplest amphiphiles and can be dissolved to high amounts in phospholipid bilayers. (c) Dilauroyl phosphatidylcholine, or in short DLPC. Phosphatidylcholines have two hydrocarbon tails and a zwitterionic headgroup. They are abundant in animal cells and the best studied model system for biological lipids. (d) Monoolein, a monoacyl glycerol with one (unsaturated) hydrocarbon tail.

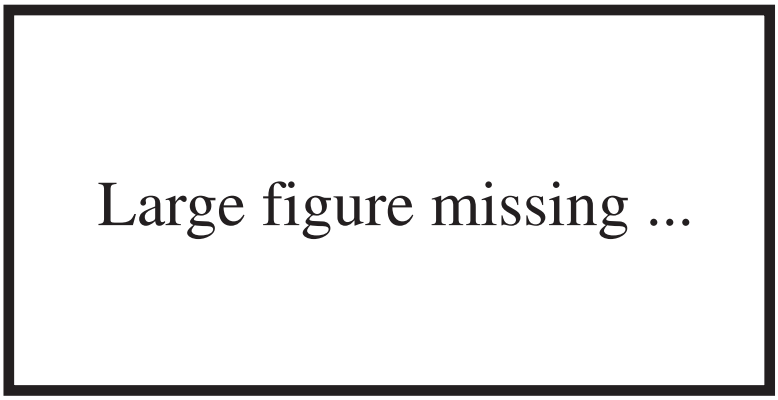

Figure 2: Self-assembly of amphiphiles: (a) in binary systems, amphiphiles self-assemble into bilayers, micelles and vesicles in order to shield the hydrophobic tails from the aqueous solvent. (b) In ternary systems, the oil-like solvent swells the hydrophobic regions. If the oil-like solvent is the majority component, inverse structures occur. In ternary systems, all interfaces are amphiphilic monolayers.

ferent control parameters: for diblock copolymers and amphiphiles, these are polymer size and solvent concentrations, respectively. Since the solvent in an amphiphilic system usually has no special physical properties by itself, its properties are mostly determined by its interfaces. This stands in marked contrast to the case of diblock copolymer systems, where the entropy of chain configurations in the regions away from the interfaces cannot be neglected in a physical description (for a review see [71] and references therein). As we will discuss in more detail below, interface descriptions have been very successful in describing the properties of amphiphilic systems (for reviews see [63, 40, 64, 104, 92]).

Amphiphilic systems can be classified according to the solvent used. A mixture of water and amphiphile is called a *binary* system, and a mixture of water, oil and amphiphile is called a *ternary* system. In binary systems, amphiphiles self-assemble into spherical, cylindrical or bilayer structure in such a way that the hydrophobic tails are shielded from the hydrophilic solvent; in ternary systems, amphiphiles self-assemble into monolayer structures in such a way that the hydrophobic tails and the hydrophilic heads face the hydrophobic and hydrophilic solvents, respectively (see Fig. 2). Irrespective of these differences, amphiphiles in binary and ternary systems assemble into similar geometries, because in both cases one deals with extended sheet-like structures (the same geometries also occur in diblock copolymer systems). At room temperature, amphiphiles in mono- and bilayers usually form a two-dimensional fluid, that is the molecular constituents show only short-ranged and no long-ranged order in the plane of the interface. Therefore the sheet-like structures in amphiphilic systems are called *fluid membranes* (in fact membrane fluidity is essential for

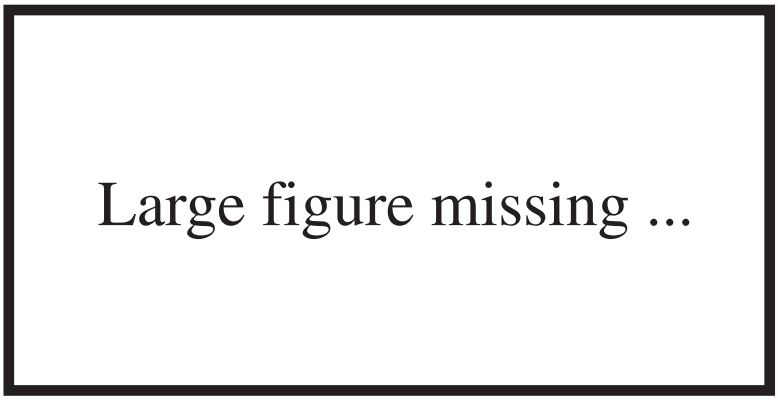

Figure 3: Geometries of self-assembled interfaces: (a) micellar (spheres), (b) hexagonal (cylinders), (c) lamellar (planes), (d) cubic bicontinuous (cubic minimal surfaces) and (e) disordered bicontinuous (random surfaces). In amphiphilic systems, mono- or bilayers are draped onto the mathematical surfaces. *Bicontinuous* means that there is one surface which spans the whole sample, thereby separating it into two disjunct yet intertwined labyrinths (like the corresponding surface, each labyrinth is connected and spans the whole sample). Note that except for (e), all surfaces are ordered and have constant mean curvature.

the functioning of the protein machinery carried by biomembranes).

Since the physics of amphiphilic systems is mostly determined by their interfaces, different geometries have comparable free energies and small changes in external variables can induce phase transitions. In particularly, for amphiphilic systems different geometries are stable for different values of concentrations and temperature. In order to achieve systematic control of amphiphilic systems, a large effort has been invested into experimentally determining the phase diagram for many important amphiphilic systems. It has been found that despite their molecular diversity, the phase behavior of amphiphilic systems follows some general rules which result from their intrinsic tendency for self-assembly into sheet-like structures. For example, for increasing amphiphile concentration one usually finds the generic phase sequence micellar disordered - micellar ordered - hexagonal - cubic bicontinuous - lamellar. *Micellar* means spherical geometry; *micellar ordered* corresponds to an ordered (usually cubic) array of spherical micelles. *Hexagonal* denotes a two-dimensional packing of cylindrical aggregates. *Bicontinuous* means that one surface partitions space into two separate labyrinths, each of which can be used to traverse space. *Cubic bicontinuous* corresponds to a space-filling arrangement of one interface, which folds onto itself in a cubic arrangement. Sometimes non-cubic spacegroups are found, but most ordered bicontinuous structures in equilibrium are cubic. In some systems, bicontinuous yet disordered phases occur, which are called *sponge phases* and *microemulsions* for binary and ternary systems, respectively. *Lamellar* cor-

responds to a one-dimensional stack of interfaces. Ordered arrangements like hexagonal or cubic symmetries can be probed by scattering techniques, and bicontinuity by diffusion experiments (e.g. using nuclear magnetic resonance). Fig. 3 tries to visualize the different interface geometries. It is the case of cubic bicontinuous phases which is the main focus of this paper.

There exists a large body of literature on the occurrence of bicontinuous phases in amphiphilic systems (for reviews see [27, 68, 103]). In Fig. 4 we show experimental phase diagrams for binary [72, 108] and ternary [59, 76] systems with the small surfactant $C_{12}E_5$ (this is the molecule shown in Fig. 1a). For the binary system, Fig. 4a, at low temperature one sees the sequence hexagonal H_1 - cubic bicontinuous V_1 - lamellar L_α with increasing amphiphile concentration. For high temperature, the hexagonal and cubic bicontinuous phases disappear, the lamellar phase L_α expands (its interfaces unbind), and for very small amphiphile concentration a sponge phase L_3 occurs. For the ternary system, Fig. 4b, we recognize the same situation again close to the binary side water-amphiphile. For equal amounts of water and oil and not too large concentration of amphiphile, that is in the lower middle of the Gibbs triangle, one sees the following phase behavior: at low temperature an emulsification failure occurs, that is the micellar disordered phase L_1 coexists with an oily excess phase. At high temperature, the emulsification failure disappears and is replaced by a microemulsion (the central, triangular one phase region). We can conclude that at low temperature, strongly curved structures prevail (H_1, L_1), while at high temperature, those structures become stable which are locally flat (L_α, L_3, microemulsion). As we will show below, this behavior can be understood using the concept of a temperature dependent spontaneous curvature: spontaneous curvature is finite at low temperature, but vanishes at high temperature. The concept of finite spontaneous curvature also offers a natural explanation for the emulsification failure at low temperature. As we will argue below, the cubic bicontinuous phase V_1 is an intermediate structure between strongly curved and locally flat. It also follows from the phase behavior described that at low temperature, stable phases tend to be ordered (H_1, V_1), while disordered phases profit from increased temperature (L_3, microemulsion). We will discuss below that the disordered phases indeed have a larger configurational entropy. In this respect, it is the lamellar phase L_α which acts as an intermediate structure.

In Fig. 5 we show experimental phase diagrams for two different lipid-water mixtures. Fig. 5a is for water and 2:1 lauric acid / dilauroyl phosphatidylcholine [110] and Fig. 5b for water and monoolein [88] (these are the molecules shown in Fig. 1b-d). Despite the molecular differences, the macroscopic phase behavior is surprisingly similar. At low temperature the membranes loose their fluidity. At intermediate temperatures, the lamellar phase is stable, and at high temperatures, it is replaced by the hexagonal phase. Whereas in the case of the surfactant $C_{12}E_5$ spontaneous curvature is finite at ambient temperatures and vanishes at high temperature, for the lipids spontaneous curvature vanishes at ambient temperatures and increases with temperature. Several cubic bicontinuous phases are stable for intermediate temperatures, in the sequence lamellar - G - D - P (here G, D and P stand for cubic bicontinuous structures which

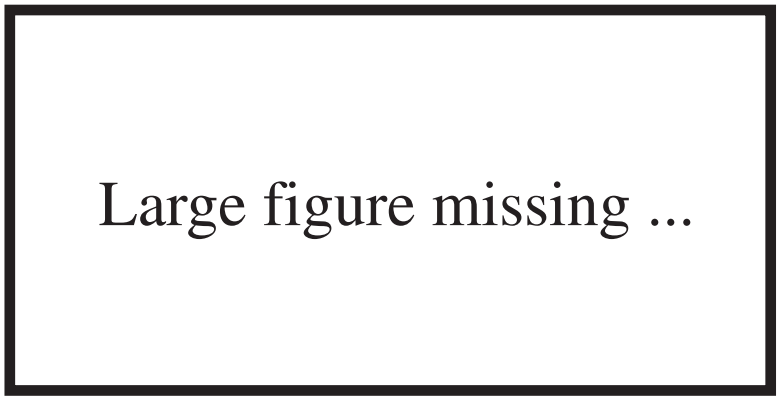

Figure 4: Experimentally determined phase behavior for the surfactant $C_{12}E_5$: binary system ($H_20/C_{12}E_5$) [108] (top) and ternary system ($H_20/C_{12}E_5/C_{14}$) [76] (bottom). In the binary system, the hexagonal phase H_1, the cubic bicontinuous phase V_1, the lamellar phase L_α, the sponge phase L_3 and the micellar phases L_1 and L_2 are stable. In the ternary system, the same phases occur close to the binary side $H_20/C_{12}E_5$. At $T_1 = 5°T$ and $T_2 = 25°T$, L_1 coexists with excess oil (emulsification failure). At $T_3 = 48°T$ (balanced temperature), a bicontinuous microemulsion is stable in the middle of the Gibbs triangle.

are discussed in more detail below) with increasing water content. The last phase in this sequence undergoes an emulsification failure, that is it coexists with an excess water phase. We will show below that this phase behavior can be explained nicely if the lipid monolayers of the cubic bicontinuous phases are modeled as parallel surfaces to a cubic minimal midsurface.

In this article, we focus on the interface description of amphiphilic systems, that is the free energy of the system is written as a functional of its interface configuration. The interface free energy is introduced in the next section (Sec. 2), and in the rest of this article we will specify this free energy expression for different instances of cubic bicontinuous phases. In each case, we will discuss the relevant geometric properties and show how they relate to the resulting free energy expressions and phase diagrams. Our starting point are *triply periodic minimal surfaces* (TPMS) in Sec. 3, a subject well-known from differential geometry. These structures are expected to occur if the amphiphilic interface is symmetric in regard to its two sides and if temperature is not too high as to destroy the ordered state. TPMS are also the reference state for their parallel surfaces and CMC-companions, which are the adequate structural models for a detailed analysis of amphiphilic monolayers in cubic bicontinuous phases. In the case that the physical interface is not symmetric in regard to its two sides (that is if spontaneous curvature exists, like usually for an amphiphilic monolayer at a water-oil interface), the relevant mathematical representations are the constant mean curvature companions of the TPMS, that is *triply periodic surfaces*

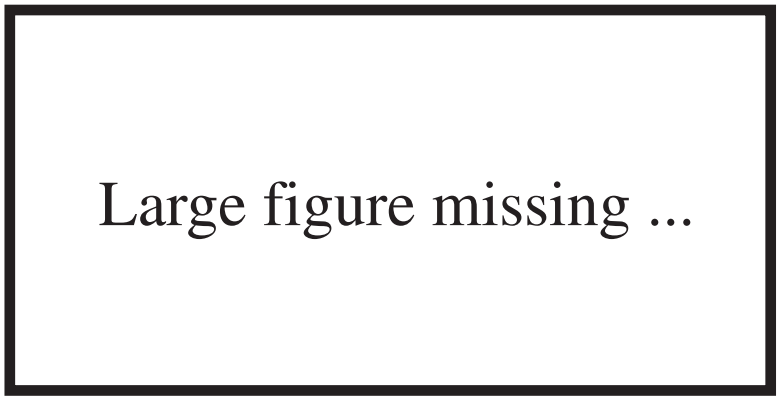

Figure 5: Experimentally determined phase behavior for lipid-water mixtures: 2:1 lauric acid / dilauroyl phosphatidylcholine [110] (top) and monoolein [88] (bottom). In both phase diagrams, one sees the sequence lamellar - cubic bicontinuous - excess water (emulsification failure) at intermediate temperatures (around $40°C$) and with increasing water concentration. In (a), G, D and P are stable. In (b), G (Ia3d) and D (Pn3m) are stable.

of constant mean curvature (CMC-surfaces) treated in Sec. 5. The case of lipid bilayers might be considered to be the composition of two such CMC-surfaces, but we will argue in Sec. 4 that in this case the relevant geometry is in fact the one of *parallel surfaces* to a TPMS. In all of these cases, we are interested in ordered structures, and therefore the main method will be minimization of the corresponding free energy functionals. This is different in Sec. 6, where we will discuss disordered bicontinuous phases, that is the sponge phases and microemulsions, which often occur at higher temperatures due to entropic effects. These structures are modeled as *random surfaces*, thus the main model here will be Gibbs distributions, in particular the theory of Gaussian random fields and Monte Carlo simulations.

2 Free energy functionals

2.1 Interface models

From the viewpoint of elasticity theory, amphiphilic interfaces with small curvatures can be considered to be thin elastic shells, which are known to have few fundamental modes of deformation: out-of-plane bending, in-plane compression and in-plane shearing [60]. However, since amphiphilic interfaces are fluid and nearly incompressible, in-plane strain is irrelevant and the most relevant deformation mode is bending. For small curvatures the free energy of an amphiphilic

interface is a function only of its geometry [8, 47]:

$$F = \int dA \left\{ \sigma + 2\kappa (H - c_0)^2 + \bar{\kappa} K \right\} \ . \tag{1}$$

Here dA denotes the differential area element and H and K mean and Gaussian curvature, respectively. The latter two follow from the two principal curvatures k_1 and k_2 as $H = (k_1 + k_2)/2$ and $K = k_1 k_2$. The three material parameters introduced in Eq. (1) define the energy scales of the corresponding changes: σ is *surface tension* and corresponds to changes in surface area, κ is *bending rigidity* and corresponds to cylindrical bending, and $\bar{\kappa}$ is *saddle-splay modulus* (or *Gaussian bending rigidity*) and corresponds to changes in topology due to the Gauss-Bonnet-theorem for closed surfaces, $\int dAK = 2\pi\chi$, where χ denotes Euler characteristic. The *spontaneous curvature* defines the reference point for bending deformations. It has to vanish for symmetric amphiphilic sheets (like lipid bilayers), but in general is finite for non-symmetric ones (like monolayers). For monolayers, it is usually a linear function of temperature, $c_0 \sim (T - T_b)$. Therefore spontaneous curvature vanishes at the balanced temperature T_b, at which solvent properties make the monolayer symmetric in regard to bending.

For amphiphilic interfaces, surface area is proportional to the number of amphiphilic molecules, thus σ can also be interpreted as a chemical potential for amphiphiles. The bending rigidity κ has to be positive, otherwise the system would become instable to spontaneous convolutions. For surfactant and lipid systems, its values are of the order of 1 and 20 $k_B T$, respectively. Surface tension σ can assume negative values (favorable chemical potential for the influx of amphiphiles), as long as bending rigidity κ exists and has a positive value, in order to prevent an instability towards proliferation of interfacial area. The value of the saddle-splay modulus $\bar{\kappa}$ is often debated, but usually it is assumed to have a small negative value. This assumption is validated by the following argument [48]: for $\sigma = 0$ and $c_0 = 0$, we can rewrite Eq. (1) as

$$F = \int dA \left\{ \frac{1}{2}\kappa_+ (k_1 + k_2)^2 + \frac{1}{2}\kappa_- (k_1 - k_2)^2 \right\} \tag{2}$$

with

$$\kappa_+ = \kappa + \frac{\bar{\kappa}}{2}, \quad \kappa_- = -\frac{\bar{\kappa}}{2} \ . \tag{3}$$

From this we conclude that the Gaussian bending rigidity has to satisfy $\kappa_+ > 0$ and $\kappa_- > 0$, that is $-2\kappa < \bar{\kappa} < 0$, otherwise the system would become unstable. For $\bar{\kappa} < -2\kappa$ ($\kappa_+ < 0$), we would get $k_1 = k_2 \to \infty$, that is many small droplets, and for $\bar{\kappa} > 0$ ($\kappa_- < 0$), we would get $k_1 = -k_2 \to \infty$, that is a minimal surface with very small lattice constant.

From the mathematical point of view, it is interesting that for $\sigma = 0$ and $c_0 = 0$, the bending energy from Eq. (1) is not only invariant under rescaling with length, but also invariant under conformal transformations in general. This has intriguing consequences for vesicles [104] (vesicles are depicted in Fig. 2, but are not subject of this article) and phase transitions in systems without spontaneous curvature (as will be discussed in Sec. 6).

Since the energy scales involved are of the order of k_BT, thermal noise is sufficient to induce shape changes. Due to thermal fluctuations on smaller length scales, the effective values for the material parameters are changed (renormalized) at larger length scales [49, 79]. It has been shown in the framework of renormalization group theory that logarithmic corrections arise due the two-dimensional nature of the amphiphilic interfaces, so that [79, 17, 7]

$$\kappa_R(l) = \kappa - \frac{3k_BT}{4\pi} \ln \frac{l}{\delta} \ , \tag{4}$$

$$\bar{\kappa}_R(l) = \bar{\kappa} + \frac{5k_BT}{6\pi} \ln \frac{l}{\delta} \tag{5}$$

where l is the length scale on which the system is analyzed and δ is a microscopic cutoff on the scale of the membrane thickness. Thus bending rigidity decreases, while Gaussian bending rigidity increases with increasing length scale l.

For the following, it is useful to introduce two dimensionless quantities which correspond to the two curvatures of a two-dimensional surface. For a structure with surface area A and volume V, the length scale V/A can be used to rescale its curvatures. In order to be able to convert easily from local to global quantities, we consider a triply periodic CMC-surface with Euler characteristic χ and integrated mean curvature $H_i = \int dAH$ per conventional (that is simple cubic) unit cell:

$$K \left(\frac{V}{A}\right)^2 = \frac{2\pi\chi V^2}{A^3} \ , \quad H \left(\frac{V}{A}\right) = \frac{H_i V}{A^2} \ . \tag{6}$$

These expressions motivate the definition of the *topology index* Γ and the *curvature index* Λ:

$$\Gamma = \left(\frac{A^{*3}}{2\pi|\chi|}\right)^{\frac{1}{2}} \ , \quad \Lambda = \frac{H_i^*}{A^{*2}} \tag{7}$$

where $A^* = A/V^{2/3}$ and $H_i^* = H_i/V^{1/3}$ are the scaled surface area and the scaled integral mean curvature per conventional unit cell, respectively. Note that these definitions can be applied to any triply periodic surface; here we used CMC-surfaces only for an heuristic motivation of the quantities defined. Both the topology index Γ and the curvature index Λ do not depend on scaling and choice of unit cell. They are universal geometrical quantities which characterize a surface in three-dimensional space. The topology index describes its porosity (the larger its value, the less holes the structure has) and its specific area content (the larger its value, the more inner surface the structure contains), and the curvature index describes how strongly the structure is curved (irrespective of the actual lattice constant). It is interesting to note that the two indices defined here correspond to the two isoperimetric ratios known from integral geometry. For a TPMS, the curvature index Λ vanishes and the topology index Γ is its most important geometric characteristic.

2.2 Ginzburg-Landau models

A different but equally powerful approach to amphiphilic interfaces is the isosurface construction (also known as phase field method), which derives a two-dimensional surface from a three-dimensional scalar field $\Phi(\mathbf{r})$. For ternary amphiphilic systems, $\Phi(\mathbf{r})$ can be interpreted as the local concentration difference between water ($\Phi = 1$) and oil ($\Phi = -1$). The position of the amphiphilic monolayer can be identified with the isosurface $\Phi(\mathbf{r}) = 0$. For binary amphiphilic systems, $\Phi(\mathbf{r})$ can be interpreted as the local concentration difference between water on different sides of a bilayer, and the isosurface $\Phi(\mathbf{r}) = 0$ marks the position of the bilayer mid-surface. In both cases, an energy functional can be defined in the spirit of a Ginzburg-Landau theory for the scalar field $\Phi(\mathbf{r})$. A reasonable choice is the Φ^6-model introduced by Gompper and Schick [39, 40]:

$$\mathcal{F}[\Phi] = \int d\mathbf{r} \ \left\{ (\Delta\Phi)^2 + g(\Phi)(\nabla\Phi)^2 + f(\Phi) \right\} \tag{8}$$

with the following choice for f and g:

$$f(\Phi) = (\Phi+1)^2(\Phi-1)^2(\Phi^2+f_0) \ , \ g(\Phi) = g_0 + g_2\Phi^2 \ . \tag{9}$$

It has been shown that this model is similar to an interface description as given in Eq. (1), and prescriptions have been given how to calculate the parameters of the interface Hamiltonian from the given Ginzburg-Landau theory [41]. Due to the invariance under $\Phi \to -\Phi$, spontaneous curvature c_0 vanishes in this model. For given model parameters (g_0, g_2, f_0), this energy functional can be minimized for its spatial degrees of freedom, and a phase diagram can be calculated as a function of model parameters by identifying the absolute minimum at every point. A reasonable choice for amphiphilic systems is $g_0 < 0$, f_0 close to 0 and g_2 not too large. Then the formation of interfaces is favored and a lamellar phase becomes stable. Calculation of the corresponding parameters of the interface model then yields $\sigma < 0$, $\kappa > 0$ and $\bar{\kappa} < 0$. Note that $\sigma < 0$ favors the formation of interfaces, and that $\bar{\kappa} < 0$ favors the lamellar phase.

3 Triply periodic minimal surfaces (TPMS)

Minimal surfaces and surfaces of constant mean curvature (see Sec. 5) in general have attracted a lot of attention both in mathematics and in physics, partially due to their intrinsic beauty, which might be considered to follow from the fact that they are solutions to variational problems [51]. It is important to note that the different fields are interested in different aspects of the same object: while for mathematicians the most central question is the existence proof for a minimal surface of interest, physicists are more interested in its representation, which can be used to derive physical properties of corresponding material systems. As Karcher and Polthier remark, outside mathematics only pictured minimal surfaces have been accepted as existent [56]. In fact this statement can also be reversed: not every structure which one can picture is necessarily

a minimal surface. In this article we consider only established minimal surfaces. As we are motivated by physical considerations, we are interested only in embedded surfaces which do not self-intersect. In regard to mathematics, our main emphasis here will be on representations, since the physical properties of amphiphilic systems follow from their spatial structure.

Minimal surfaces are surfaces with $H = 0$ everywhere. If one varies a surface with a normal displacement $\delta\phi(u, v)$ (where u and v are the internal coordinates of the surface), it can be shown that the change in surface area is $\Delta A = 2\delta \int dA\phi(u, v)H(u, v) + O(\delta^2)$ [54], that is a minimal surface is a stationary surface for variations of surface area. Therefore surfaces under surface tension (like soap films), which try to minimize surface area, form minimal surfaces. Here we consider surfaces which are dominated by bending rigidity rather than by surface tension. However, for vanishing spontaneous curvature the resulting structures also correspond to minimal surfaces. Eq. (1) explains why: these surfaces have to minimize $\int dAH^2$ (they are so-called *Willmore surfaces*), and minimal surfaces are a special case of Willmore surfaces, since $H = 0$ is a trivial minimization of this functional.

If mean curvature $H = (k_1+k_2)/2 = 0$, then Gaussian curvature $K = k_1k_2 = -k_1^2 \leq 0$. Thus minimal surfaces are everywhere either saddle-like or flat, and nowhere convex. In fact it can be shown that the flat points with $k_1 = k_2 = 0$ are isolated. Moreover it follows from $K \leq 0$ that minimal surfaces without boundaries cannot be compact [54]. Until 1983, only two embedded minimal surfaces were known which are non-periodic: the plane and the catenoid. Then a new surface of this type was found, the Costa-surfaces, which from the distance looks like the union of a plane and a catenoid [56]. Today some more surfaces of this type are known, but the majority of all embedded minimal surfaces without boundaries are in fact periodic. There is only one simply-periodic minimal surface, the helicoid, and there are some doubly-periodic surfaces, with the Scherk-surface being most prominent. The majority of all known periodic minimal surfaces is triply-periodic. Here we will focus on cubic minimal surfaces and their physical realizations, which are cubic bicontinuous structures.

The best known triply periodic minimal surface (TPMS) is the P-surface found by Schwarz in 1867 and depicted in Fig. 3d. Schwarz and his students found 5 TPMS, including the cubic cases P, C(P) and D. Until 1970 no more examples were found, then Schoen described 13 more [96], including the cubic cases G, F-RD, I-WP, O,C-TO and C(D). He proved the existence of G by providing an explicit (Weierstrass) representation, and the existence of the others was proven in 1989 by Karcher [55]. More TPMS have been discovered by Fischer and Koch [23, 57] and others, and today many more can be generated by making controlled modifications to computer models of known TPMS, a method which was pioneered by Polthier and Karcher [56]. However, these surfaces tend to be rather complicated, and we will show below that only the simple (as quantified by the topology index) TPMS are relevant for amphiphilic systems. In Fig. 6 we show visualizations of 10 different TPMS with cubic symmetry. There representations have been obtained from the Φ^6-Ginzburg-Landau theory as will be explained below. For some of these structures, we also show

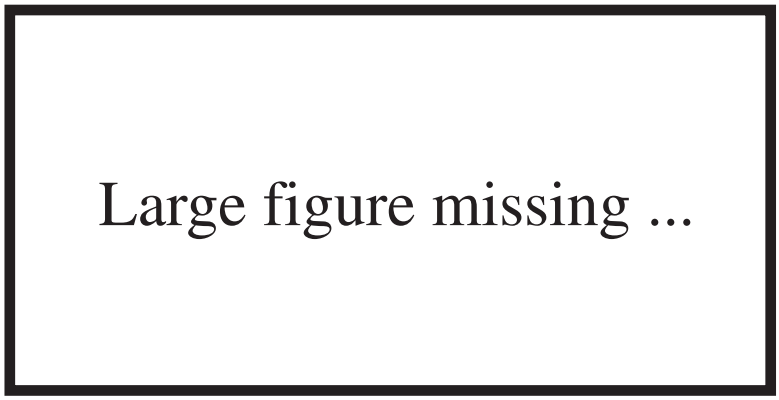

Figure 6: Visualizations of 10 different cubic minimal surfaces. Every triply periodic surface divides space into two labyrinths, which in some cases are represented here by skeletal graphs. D and G are the basis for the double-diamond structure and the gyroid, respectively, which often occur in physical systems.

line-like representations of the two labyrinths defined by the surface (*skeletal graphs*). For example, in the case of the Schwarz P-surface, the two skeletal graphs are the edges of the surrounding cube and the three lines through the origin.

Different methods can be used to obtain representations of TPMS. Until recently, the main method were the Weierstrass representation formulae. For the cubic TPMS, they are known for P, D and G [25, 26] as well as for I-WP [62, 12]. For each of these TPMS, a fundamental domain can be identified, so that the rest of the surface follows by replicating it with the appropriate space group symmetries ($Im\bar{3}m$, $Pn\bar{3}m$, $Ia\bar{3}d$ and $Im\bar{3}m$, respectively). The Weierstrass representation is a conformal mapping of certain complicated regions within the complex plane onto the fundamental domain:

$$(x_1, x_2, x_3) = Re \int_0^{u+iv} dz\ R(z)\ (1 - z^2, i(1 + z^2), 2z) \tag{10}$$

where (u, v) are the internal (and conformal) coordinates of the minimal surface. The Weierstrass mapping can be understood as the inversion of the following composition: first the surface is mapped onto the unit sphere via its normal, and then the unit sphere is mapped onto the complex plane by stereographic projection. The geometrical properties of a surface follow from the Weierstrass representation as

$$dA(z) = |R(z)|^2\ (1 + |z|^2)^2\ dudv,\ H(z) = 0,\ K(z) = \frac{-4}{|R(z)|^2(1 + |z|^2)^4} \tag{11}$$

with $z = u + iv$. Obviously the (isolated) poles of $R(z)$ correspond to the flat points ($K = 0$) of the minimal surface. Only few choices of $R(z)$ yield embedded

	χ	A^*	Γ
G	-8	$3(1+k_1^2)/2k_1 = 3.091444$	0.766668
D	-16	$3/k_1 = 3.837785$	0.749844
I-WP	-12	$2\sqrt{3} = 3.464102$	0.742515
P	-4	$3k_1 = 2.345103$	0.716346
C(P)	-16	$3/k_2 = 3.510478$	0.655993

Table 1: Euler characteristic χ, scaled surface area A^* in the conventional unit cell and topology index $\Gamma = ({A^*}^3/2\pi|\chi|)^{1/2}$ for those TPMS, for which exact results are known from Weierstrass representations. Here $k_1 = K(1/2)/K(\sqrt{3}/2)$ where $K(k)$ is the complete elliptic integral of the first kind, and $k_2 = K(1/\sqrt{3})/K(\sqrt{2/3})$. Note that often a unit cell is chosen for D which is the eighth part of the one chosen here; then one has $\chi = -2$ and $A^* = 1.918893$.

minimal surfaces. The ones for D and P have been known since the 19th century from the work of Schwarz: for D it is $R(z) = (z^8 - 14z^4 + 1)^{-\frac{1}{2}}$. P follows simply by the Bonnet transformation $R(z) \to e^{i\theta}R(z)$ with $\theta = 90°$. Eq. (11) implies that P and D have the same metric and the same distribution of Gaussian curvature. However, since they map differently into embedding space, they have different space groups and lattice constants. The gyroid G was discovered in 1970 by Schoen [96] as another Bonnet transformation of D, with $\theta = 38.015°$. The Weierstrass representation for I-WP was found only recently [62, 12]. If one of its poles is chosen to be at infinity, one has $R(z) = (z(z^4+1))^{-\frac{2}{3}}$. In Tab. 1 we give exact results for geometrical properties which have been derived from Weierstrass representations (although for C(P) no Weierstrass representation is known, these values can be derived from its complementary relationship to P). Note that the topology index Γ establishes the hierarchy G - D - P within this Bonnet family. This sequence corresponds to the connectivity of the labyrinths defined by the TPMS: G has 3-fold, D 4-fold and P 6-fold coordination, since higher coordinated structures have more holes.

It is interesting to note that the identification of these structures in material systems is a difficult enterprise, which depends on the availability of suitable representations. Physical representations of TPMS have been built since the 19th century, using soap films draped onto wire skeletons (without the wire skeletons surface tension would shrink these structures into collapse). In 1967 Luzzati and Spegt noted that certain phases in lipid systems are cubic bicontinuous [67], but it was only in 1976 that Sciven suggested the relevance of TPMS as structural models for cubic bicontinuous phases [102]. The Luzzati-Spegt structure was later identified with the gyroid structure G, and the diamond structure D was identified both in lipid [65] and diblock copolymer systems [114]. For diblock copolymer systems, the gyroid structure G was identified in 1994 [45], and little later it was noted that earlier identifications of cubic bicontinuous phases in diblock copolymer systems often mistook the gyroid structure G for the diamond structure D [46] (in fact, for diblock copolymer systems one should rather use

the terms *double diamond* and *double gyroid*, since in this case two interfaces are arranged around the corresponding TPMS). Today, the structures G, D, P and I-WP seem to be non-ambiguously identified in amphiphilic system, with experimental evidence based mainly on small angle scattering experiments, electron transmission microscopy, and swelling and diffusion experiments [27, 68, 103].

Apart from the cases G, D, P and I-WP given above, no more Weierstrass representations are known for cubic TPMS, so for all other cases numerical methods have to be used. For example, the *Surface Evolver* is a software package written by Brakke which allows to minimize triangulated surfaces for different energy functionals (compare Sec. 8). Here we discuss the method of constructing the isosurfaces of a scalar field $\Phi(\mathbf{r})$, as introduced in Sec. 2.2. For our purpose, the usefulness of this model lies in its rugged energy landscape, which means that many more local minima exist than the absolute minima corresponding to the lamellar phase. In physical terms, these additional minima correspond to modulated phases which are metastable. If started with suitable initial conditions, the minimization procedure therefore yields representations which can be used to characterize the structural properties of these phases. Therefore this model has been used repeatedly in order to investigate bicontinuous cubic phases [41, 42, 43, 97]. In particularly, it has been found that the resulting representations are very close to TPMS [42, 43]. This finding can be explained as follows [97]: for a triply-periodic cubic structure, the free energy per unit volume $f = F/V$ follows from the interface description of Eq. (1) as

$$f = \frac{1}{a}\left(\sigma A^*\right) + \frac{1}{a^3}\left(2\kappa \int dA\ H^2 + 2\bar{\kappa}\pi\chi\right) \tag{12}$$

where a is the lattice constant of the conventional unit cell. Both terms in brackets are scale invariant, that is they do not depend on the lattice constant a. Since for the Ginzburg-Landau model at hand the first and second term in brackets is negative and positive, respectively (compare Sec. 2.2), a balance exists between the negative surface tension term, which favors small values of a, and the positive curvature contributions, which favors large a. If we make the assumption that the minimization problem can be decomposed in two independent minimizations, one for lattice constant a and one for the shape, we can first minimize f for a while considering A^* and $\int dA\ H^2$ to be constant:

$$a_{min} = \left(\frac{6\pi\bar{\kappa}\chi + 6\kappa\int dAH^2}{|\sigma|A^*}\right)^{\frac{1}{2}}, \quad f_{min} = -\left(\frac{4}{27}\right)^{\frac{1}{2}}\left(\frac{(|\sigma|A^*)^3}{2\bar{\kappa}\pi\chi + 2\kappa\int dAH^2}\right)^{\frac{1}{2}} \tag{13}$$

Similar mechanisms are always at work in amphiphilic systems and explain why in contrast to surface tension, bending rigidity does not necessitate the presence of a scaffold (like a wire skeleton for soap films) to prevent collapse. In a second step, we now minimize f_{min} for shape. If we assume A^* to be constant, we have reduced our problem to the Willmore problem, and this is why minimal surfaces with $H = 0$ appear in the framework of the Φ^6-theory. The final free-energy

density can be written as

$$f_{min} = -\left(\frac{4}{27}\right)^{\frac{1}{2}} \left(\frac{|\sigma|^3}{|\bar{\kappa}|}\right)^{\frac{1}{2}} \Gamma \tag{14}$$

where Γ is the topology index defined in Eq. (7). We conclude that the stability of the different TPMS is governed by their topology indices and that the most favorable bicontinuous cubic phase is the gyroid G since it has the largest value for Γ (compare Tab. 1). Although this conclusion is based on some assumptions, it is corroborated by a detailed numerical analysis [97].

In order to obtain representations for a large list of TPMS, we used the Fourier approach and the theories of black and white space groups to obtain TPMS as local minima of the Φ^6-theory [97]. Black and white space groups are also known as magnetic or Shubnikov space groups and lead to a crystallographic classification of TPMS [23, 24]. Implementation of black and white symmetries leads to a considerable reduction in the degrees of freedoms of the Fourier series. Therefore this method is computationally cheap and its results are easy to document and to reuse. A triply periodic surface partitions space into two labyrinths, which can be considered to be colored black and white. In the framework of the Ginzburg-Landau theory, black and white correspond to $\Phi > 0$ and $\Phi < 0$, respectively. The surface is called *balanced* if there exists an Euclidean transformation α which maps the white labyrinth onto the black one and vice versa; otherwise it is called *non-balanced*. Examples for non-balanced surfaces are I-WP and F-RD, and the Fourier approach for the corresponding structure follows the usual rules for the respective space group [106]. However, if the surface is balanced, the structure is characterized by *two* space groups: if the colored structure has space group $\mathcal{H}$, the uncolored structure has space group $\mathcal{G} = \mathcal{H} \otimes \{1, \alpha\}$. $\mathcal{H}$ contains all symmetry operations of $\mathcal{G}$ that do not interchange the two labyrinths. It is a subgroup of $\mathcal{G}$ of index 2, that is the quotient group is isomorphic to the cyclic group of order 2, $\mathcal{G}/\mathcal{H} \cong \mathbb{Z}_2 \cong \{1, \alpha\}$. For example, for the balanced cubic surface defined by $\cos x + \cos y + \cos z = 0$, the operation interchanging the two labyrinth is the translation by half a body diagonal, and we have $\mathcal{H} = Pm\bar{3}m$ and $\mathcal{G} = Im\bar{3}m$.

Since $\mathcal{H}$ has index 2 in $\mathcal{G}$, it follows from the theorem of Hermann [105] that $\mathcal{H}$ has either the same point group or the same Bravais lattice as $\mathcal{G}$. If $\mathcal{H}$ and $\mathcal{G}$ have the same point group, their Bravais lattices have to be different. Thus the Euclidean operation α has to be a translation which extends one cubic Bravais-lattice into another. For the cubic system, there are only three different Bravais lattices (simple cubic P, body-centered cubic I and face-centered cubic F), and only two possibilities to extend one into the other by a translation $\mathbf{t}_\alpha$: for $\mathbf{t}_\alpha = a(\mathbf{x} + \mathbf{y} + \mathbf{z})/2$ a P-lattice becomes a I-lattice, and for $\mathbf{t}_\alpha = a\mathbf{x}/2$ a F-lattice becomes a P-lattice. The condition $\Phi(\mathbf{r} + \mathbf{t}_\alpha) = -\Phi(\mathbf{r})$ leads to reflection conditions for the reciprocal vectors. For Miller indices (h, k, l), one finds $h + k + l = 2n + 1$ for $P \to I$, and $h, k, l = 2n + 1$ for $F \to P$. Note that these reflection conditions are similar to the well-known ones $h + k + l = 2n$ for I and $h + k, h + l, k + l = 2n$ for F. The P-surface has space group $Pm\bar{3}m$, but

	$\mathcal{H}$	$\mathcal{G}$	$\mathcal{H} \rightarrow \mathcal{G}$	nodal approximations
G	$I4_132$	$Ia\bar{3}d$	$432 \rightarrow m\bar{3}m$	$\sin(x)\cos(y) + \sin(y)\cos(z) + \sin(z)\cos(x)$
D	$Fd\bar{3}m$	$Pn\bar{3}m$	$F \rightarrow P$	$\cos(x-y)\cos(z) + \sin(x+y)\sin(z)$
P	$Pm\bar{3}m$	$Im\bar{3}m$	$P \rightarrow I$	$\cos(x) + \cos(y) + \cos(z)$
C(P)	$Pm\bar{3}m$	$Im\bar{3}m$	$P \rightarrow I$	$\cos(x) + \cos(y) + \cos(z) + 3\cos(x)\cos(y)\cos(z)$

Table 2: Group - subgroup pairs $\mathcal{G} - \mathcal{H}$, the relation $\mathcal{H} \rightarrow \mathcal{G}$ between them and nodal approximations for some balanced cubic minimal surfaces. $\mathcal{G}$ and $\mathcal{H}$ differ either in Bravais lattice or in point group, but not in both. Nodal approximations only consider the space group information given by $\mathcal{G} - \mathcal{H}$. For the simple cases, the first mode of the corresponding Fourier series is sufficient to obtain the correct topology.

	$\mathcal{G}$	nodal approximations
I-WP	$Im\bar{3}m$	$2[\cos(x)\cos(y) + \cos(y)\cos(z) + \cos(z)\cos(x)]$ $-[\cos(2x) + \cos(2y) + \cos(2z)]$
F-RD	$Fm\bar{3}m$	$4\cos(x)\cos(y)\cos(z)$ $-[\cos(2x)\cos(2y) + \cos(2y)\cos(2z) + \cos(2z)\cos(2x)]$

Table 3: Nodal approximations for some non-balanced cubic minimal surfaces, for which $\mathcal{H} \equiv \mathcal{G}$. In these cases, more than one mode is needed.

a black and white symmetry with supergroup $Im\bar{3}m$, therefore it is an example for the case $P \rightarrow I$. Thus we have $h + k + l = 2n + 1$ and the first Fourier mode is $(1, 0, 0)$. Note that the double P structure, which one would expect for a diblock copolymer system, has no black and white symmetry, but space group $Im\bar{3}m$, thus one has $h + k + l = 2n$ and the first mode is $(1, 1, 0)$.

If $\mathcal{H}$ and $\mathcal{G}$ have the same Bravais lattice, their point groups have to be different. Thus the Euclidean operation α has to be a point group operation which extends one cubic point group into another one. There are five cubic point groups and six ways to extend one of them into another by some P_α. The condition $\Phi(P_\alpha \mathbf{r}) = -\Phi(\mathbf{r})$ leads to more complicated rules than in the case of identical points groups [97]. However, there are few relevant examples from this class, the most interesting one being the gyroid G, where P_α is the inversion and the resulting rules are rather simple again (the even part of the Fourier series vanishes).

Fischer and Koch have completely enumerated all 34 cubic group-subgroup pairs $\mathcal{G} - \mathcal{H}$ with index 2 which are compatible with cubic balanced TPMS [23]. Although there is no way to completely enumerate all TPMS belonging to a given pair $\mathcal{G} - \mathcal{H}$ in general, this is possible for a certain subset, that is for all cubic balanced TPMS which contain straight lines which form a three-dimensional network [23]. This list reads P, C(P), D, C(D), S and C(Y). In our work, we implemented Fourier series for these structures as well as for the

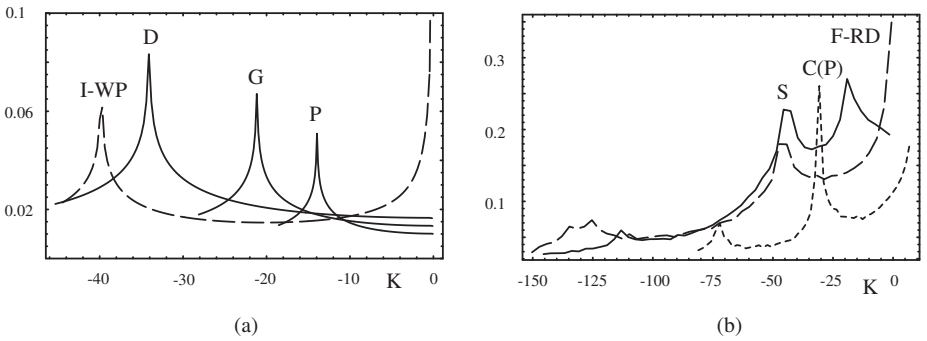

Figure 7: Distribution $f(K)$ of Gaussian curvature K over the cubic minimal surfaces investigated in the framework of the Φ^6-model. (a) For the structure G, D, P and I-WP, the data is obtained from their exact Weierstrass representations; the agreement with the numerical results from the Φ^6-model is good (not shown). (b) For the structures F-RD, S and C(P), no Weierstrass representation is known, and the data is obtained from the Φ^6-model.

gyroid G (which is balanced, but does not contain any straight lines) and the non-balanced structures I-WP and F-RD. In some cases like G, D and P, the first mode of the Fourier ansatz implementing the correct black and white symmetry is already sufficient to obtain a representation which is topologically correct (*nodal approximation*). In all other cases investigated, the addition of one more mode (with the relative weight fixed by visual inspection) is sufficient. Nodal approximations for bicontinuous structures have been discussed first by von Schnering and Nesper [115]. In Tab. 2 and Tab. 3 we give nodal approximations and the corresponding space group information for some of the balanced and non-balanced structures investigated.

Implementing the complete Fourier series and numerically minimizing the Φ^6-functional from Eq. (8) with nodal approximations as initial conditions, we arrived at *improved nodal approximations* which were tabulated in Ref. [97] with up to six Fourier modes. The isosurface construction is easily implemented using the marching cube algorithm. The resulting triangulations can then be used to investigate geometrical properties of these surfaces. In particular, widely used mathematics programs (like Mathematica, Maple or Matlab) can be easily used to obtain useful representations of TPMS from (improved) nodal approximations. Our numerical work shows that the six modes of the improved nodal approximations are sufficient to decrease the deviation of the curvature properties from the real TPMS by one order of magnitude compared to the nodal approximations. Also we measured for the first time the distribution $f(K) = \int dA(u,v)\ \delta(K - K(u,v))$ of Gaussian curvature K over the surfaces. For this purpose, we used up to 100 Fourier modes. The distributions $f(K)$ for different structures are plotted in Fig. 7. In the cases for which Weierstrass

	G, D, P	I-WP	S	F-RD	C(P)
Δ	0.218702	0.482666	0.586079	0.649801	0.842022

Table 4: Variance Δ of the distributions of Gaussian curvature $f(K)$. The values for Δ are the same for G, D and P due to the existence of a Bonnet-transformation between them.

representations are known, the same data has been derived from the exact representations, and the resulting agreement was very good. In general, we found that the surfaces C(D), C(P), F-RD, S and C(Y), for which no Weierstrass representations are known, are much more complicated than the cases G, D, P and I-WP. This is evidenced by larger values of the topology index Γ, multi-modal distributions $f(K)$ of Gaussian curvature K, and the larger widths of these distributions. The latter property can be quantified by defining a dimensionless variance

$$\Delta = \frac{\langle (K - \langle K \rangle)^2 \rangle}{\langle K \rangle^2} \tag{15}$$

where $\langle \dots \rangle$ means area average. In Tab. 4 we give the variance Δ of the different distributions. Its value is the same for G, D and P due to the existence of a Bonnet-transformation between them. This means that G, D and P have the narrowest distribution of K (they are most uniformly curved), and all other structures have a considerably wider one, with I-WP being the next best structure.

4 Parallel surfaces

We now consider the case of cubic bicontinuous phases in lipid-water mixtures. The two examples for the experimental phase behavior of such systems given in Fig. 5 show obvious similarities, and we will show now that a theoretical description can nicely explain these [99, 100]. It has been shown by a thorough analysis of electron density maps derived from X-ray data that the mid-surfaces of the cubic bicontinuous structures in these systems are very close to minimal surfaces [68]. Indeed if one considers the lipid bilayer as one entity, it has no spontaneous curvature by symmetry and one expects a minimal surface shape for the midsurface. Each of the two monolayers of the bilayer has unequal sides and therefore finite spontaneous curvature. For lipids monolayers, spontaneous curvature increases towards the water side as a linear function of temperature. From the interface point of view, one expects each monolayer to form a CMC-surface. However, then the distance to the minimal mid-surface would vary with position and the amphiphilic tails would have to stretch in order to fill the internal space of the membrane [3, 10]. It can be shown in the framework of a simple microscopic model that the relative importance of stretching to bending contributions to the free energy of the bilayer scales as $(a/\delta)^2$, where a is lattice constant and δ is tail length [100]. Therefore stretching is prohibitively

expensive and the two monolayers do not form CMC-surfaces as expected from the curvature energy of Eq. (1), but rather parallel surfaces to the minimal mid-surface. The free energy of the cubic bicontinuous phases then follows by specifying Eq. (1) with spontaneous curvature for two monolayers which are parallel surfaces to a given TPMS. Since the parallel surface geometry does not allow to completely relax the bending energy, the overall structure is called *frustrated* [3, 10, 20].

In principle, the analysis in the framework of the parallel surface model is rather simple, since there exist exact formulae which express the geometrical properties of the parallel surface as a function of the geometrical properties of the minimal surface:

$$dA^\delta = dA\ (1 + K\delta^2)\ , H^\delta = \frac{-K\delta}{1 + K\delta^2}\ , K^\delta = \frac{K}{1 + K\delta^2} \tag{16}$$

where δ is the distance between the two surfaces (that is amphiphilic chain length). Note that these formulae are an extension of Steiner's theorem from integral geometry to non-convex bodies, which is valid as long as the distance δ is smaller than the smallest radius of curvature of the surface (otherwise the surface will self-intersect). Since mean curvature H vanishes on the reference surface, the bending energy now becomes a function only of its Gaussian curvature K. However, as we have seen above, K is distributed over the TPMS in a non-trivial way, which makes the detailed analysis rather complicated. Nevertheless, one central conclusion can be already made at this point: using Eq. (16) in Eq. (1) leads to an effective curvature energy for the lipid bilayer (to second order in δ) [85]

$$F_{bi} = \int dA \left\{ 4c_0^2\delta^2\kappa + (2\bar{\kappa} + 8c_0\delta\kappa + 4c_0^2\delta^2\kappa)K + 4\kappa\delta^2K^2 \right\}\ . \tag{17}$$

Thus we see that although effective spontaneous curvature vanishes due to the bilayer symmetry, the effective saddle-splay modulus, $\bar{\kappa}_{bi} = 2\bar{\kappa} + 8c_0\delta\kappa + O(\delta^2)$, is corrected to higher positive values due to the presence of the monolayer spontaneous curvature c_0. We conclude that as long as $c_0\delta \gtrsim -\bar{\kappa}/4\kappa$, the bicontinuous cubic phases are favored over the lamellar phase, since the preferred curvature of the monolayers translates into a topological advantage of saddle-type bilayer structures. We also see that the correction term in $\bar{\kappa}_{bi}$ is linear in c_0 and therefore in temperature T. Therefore bicontinuous phases become more favorable with increasing temperature in general (compare also Sec. 6 on disordered bicontinuous structures).

For a detailed analysis of cubic bicontinuous phases made from bilayers, we first note that the volume fraction of the lipid tails (the hydrocarbon volume fraction, which for simplicity we identify with the lipid volume fraction, since the lipid heads are rather small) can be calculated as

$$v = \frac{1}{a^3}\int_{-\delta}^{\delta} d\delta' \int dA^{\delta'} = 2A^* \left(\frac{\delta}{a}\right) + \frac{4\pi}{3}\chi\left(\frac{\delta}{a}\right)^3 \tag{18}$$

where again we have used the Gauss-Bonnet theorem. Eq. (18) can be inverted to give a/δ, the lattice constant a in units of the chain length δ, as a function

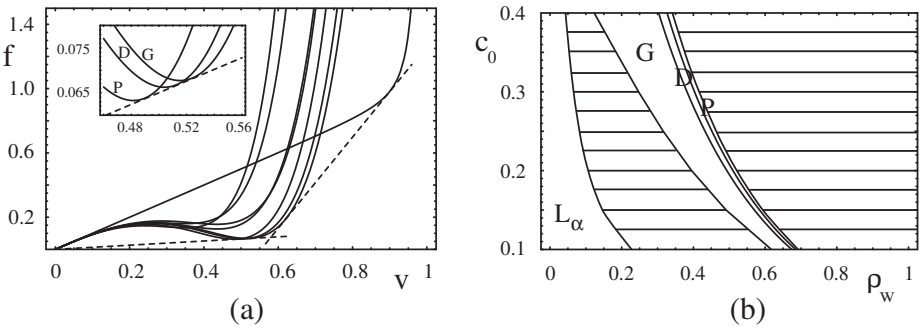

Figure 8: For cubic bicontinuous phases in lipid-water mixtures, the lipid monolayers can be modeled as parallel surfaces to a minimal mid-surface. (a) Free energy densities f as a function of lipid volume fraction v for several cubic bicontinuous phases and the lamellar phase. (b) Theoretical phase diagram as a function of water volume fraction and (dimensionless) spontaneous curvature.

of hydrocarbon volume v. For small v we find

$$\frac{a}{\delta} = \frac{2A^*}{v}\left(1 + \frac{1}{12\,\Gamma^2}v^2 + \mathcal{O}(v^4)\right) \ . \tag{19}$$

and one can check numerically that $a/\delta = 2A^*/v$ is an excellent approximation for $v \lesssim 0.8$. For larger values of v, the surfaces begin to self-intersect and our model becomes unphysical. Combining Eq. (1) and Eq. (16) yields for the bending energy per unit volume of the two monolayers (we use a factor $\delta/4\kappa c_0^2$ to write this expression dimensionless and a factor δ to write c_0 dimensionless)

$$\begin{aligned} f = v\,\Big\{ \int \frac{dA^*}{A^*}\left(1 - \Xi(K^*)\left(\frac{v}{\Gamma}\right)^2\right)^{-1} \\ \times \left(1 - \frac{1+c_0}{c_0}\Xi(K^*)\left(\frac{v}{\Gamma}\right)^2\right)^2 + \frac{r}{4c_0^2}\left(\frac{v}{\Gamma}\right)^2 \Big\} \end{aligned} \tag{20}$$

where $K^* = Ka^2$ is scaled Gaussian curvature, δ/a has been replaced by $v/2A^*$, $\Xi(K^*)$ has been defined as $K^*A^*/8\pi\chi$ (this can be considered to be a local analogue of Γ^2), and r as $-\kappa/2\bar{\kappa}$ ($0 \le r \le 1$ due to the restrictions on $\bar{\kappa}$). The free-energy density f now is a function of lipid volume fraction v, spontaneous curvature c_0, the ratio r of the two bending constants, and the distribution $f(K)$ of Gaussian curvature K. The (numerical) evaluation of this expression is only possible with the knowledge of the $f(K)$ for all TPMS of interest, which have been numerically obtained in Ref. [97] as described above.

In the limit of a planar mid-surface (lamellar phase), Eq. (20) simplifies to $f = v$ - the larger the lipid volume fraction, the more frustrated bending energy per volume accumulates. For a full analysis, one also has to include the effect

of thermal fluctuations. For the lamellar phase, they lead to a steric repulsion between the interfaces, which lead to an additional term $\sim v^3/(1-v)^2$ for the lamellar phase. For the cubic bicontinuous phases, steric repulsion is irrelevant since the lateral restriction on the scale of a lattice constant leads only to small perpendicular excursions. However, here the renormalization of the saddle splay modulus $\bar{\kappa}$ becomes relevant, and the formula given in Eq. (5) has to be incorporated. The renormalization of bending rigidity κ and spontaneous curvature c_0 is irrelevant here, since thermal fluctuations occur mainly on the level of the lipid bilayer, for which mean curvature H vanishes. For the lamellar phase, Gaussian curvature K vanishes as well, and the renormalization of all material parameters is irrelevant. Putting everything together, we can numerically calculate phase diagrams from the free energy densities of the different phases by using the Maxwell construction (construction of convex hull). In Fig. 8 we show both the free energy densities as a function of lipid volume fraction v (for fixed spontaneous curvature) and the theoretical phase diagram as a function of water volume fraction and spontaneous curvature. The main results are in excellent agreement with the experimental phase diagram shown in Fig. 5: from the many TPMS considered, only G, D and P are stable, their regions of stability have the shape of shifted parabolae, and they occur in the sequence L - G - D - P - emulsification failure. These results can be understood as follows: G, D and P can achieve the least frustration since they have the narrowest distribution of Gaussian curvature as measured by the variance Δ given in Tab. 4. This prediction has been stated before by Helfrich and Rennschuh [50], but at that time hardly any data was known to support it. The lipid volume fraction at which they achieve this can be estimated by setting the dimensionless mean curvature averaged over the parallel surface

$$\langle H^\delta \rangle_\delta \delta = \frac{\int dA^\delta \; H^\delta \delta}{\int dA^\delta} = \frac{(v/\Gamma)^2}{4-(v/\Gamma)^2} \tag{21}$$

equal to the spontaneous curvature c_0. Therefore c_0 as a function of v essentially scales as $\sim (1-\rho_W)^2/\Gamma^2$, where $\rho_W = 1-v$ is the water volume fraction. This explains the characteristic shape of the bicontinuous stability regions in both the theoretical and experimental phase diagrams. Note that at high temperature, that is large spontaneous curvature, eventually the hexagonal phase will become stable, which cannot be treated in the framework presented here. The optimal lipid volume fraction v follows from Eq. (21) as

$$v = \left(\frac{4c_0}{1+c_0} \right)^{\frac{1}{2}} \; \Gamma \; . \tag{22}$$

Therefore the structures G, D and P become stable in the sequence of their geometry index Γ, that is as G - D - P. If the water content corresponds to a average curvature of P which is larger than the optimal (spontaneous) curvature, some of the water is simply expelled from the structure, in order to keep the optimal curvature (emulsification failure). Finally it should be noted that the Bonnet-transformation connecting G, D and P causes the three structures to be

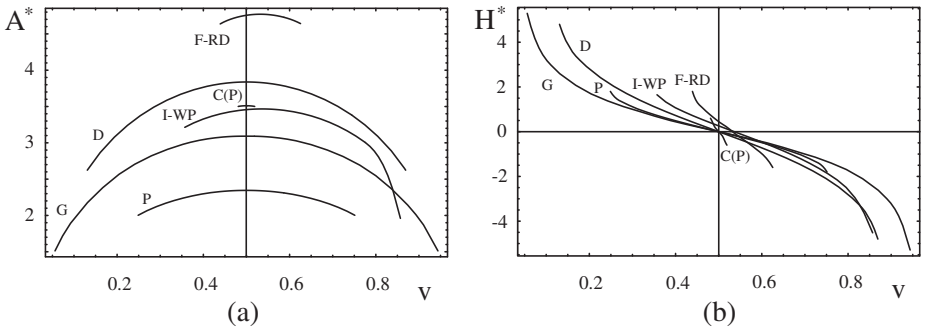

Figure 9: Geometrical data for triply periodic surfaces of constant mean curvature: (a) scaled surface area A^* and (b) scaled mean curvature H^* as a function of volume fraction v. The two branches are symmetrical for G, D, P and C(P) since their minimal surface members are balanced.

stable along a triple line (see inset of Fig. 8). This means that the stability of D and P is very delicate and can easily be destroyed by additional physical effects. Therefore we conclude that in the framework of our interfacial approach, from all TPMS considered the gyroid G is the only phase which has a robust stability in lipid-water mixtures, since among the phases with favorable distribution of Gaussian curvature, its geometrical properties are closest to the ones of the lamellar phase.

5 Surfaces of constant mean curvature (CMC)

Surfaces of constant mean curvature (CMC-surfaces) have $H = const$ everywhere, so minimal surfaces are a special case of CMC-surfaces. In contrast to minimal surfaces, CMC-surfaces with finite H can be compact, but the only CMC-surface which is compact and embedded is the sphere (for a long time, the sphere was believed to be the only compact CMC-surface, but in 1986 Wente found the first CMC-torus). Non-compact embedded CMC-surfaces are cylinder and unduloid, and all other known CMC-surfaces are doubly or triply periodic.

CMC-surfaces are solutions to the variational problem of minimal surface area under a volume constraint. This can be shown as follows: we first introduce a Lagrange parameter for volume, that is pressure p. The corresponding energy is $-pV$. For normal variations $\delta\phi(u,v)$, we have $\Delta F = 2\delta\sigma \int dA\phi(u,v)H(u,v) - p\delta \int dA\phi(u,v) + O(\delta^2)$. If the surface is required to be stationary in regard to variations in δ, we obtain the Laplace equation $H = p/2\sigma$ and H is constant over the whole surface. This explains why soap bubbles and liquid droplets are spheres (respectively spherical caps when bound by a surface). In amphiphilic systems, CMC-surface arise in the presence of spontaneous curvature: like minimal surfaces minimize the Willmore functional $\int dAH^2$, CMC-surfaces with

	G	D	I-WP	P	F-RD	C(P)
measured	0.2191	0.1411	0.1385	0.2117	0.0665	0.0466
approximation	0.1901	0.1465	0.1592	0.2188	0.0906	0.1226

Table 5: Values for $c = dv(H^*)/dH^*|_{H^*=0}$, where $v(H^*)$ is the volume fraction of one of the two labyrinths for the corresponding family of surfaces of constant mean curvature. The measured values follow from our spline interpolation of the numerical data of Ref. [2]. In the second row we give $-{A_0}^2/2\pi\chi$, a new estimate for c derived in the text.

$H = c_0$ minimize the functional $\int dA(H - c_0)^2$. In any case, since H is constant over the surface, surface area and volume now vary in the same way, and we have $dA/dV = 2H$.

All simple TPMS which are of interest for physical reasons are members of a family of CMC-surfaces [55]. Each of these families consists of two branches, corresponding to positive and negative mean curvatures, which are separated by the minimal surface member. Like the minimal surface member, each of the the triply periodic CMC-surfaces of the family partitions space into two intertwined, yet separate labyrinths, with volume fractions v and $1 - v$. Each family of CMC-surfaces, and therefore the volume fractions of the two labyrinths and the surface area A, is parametrized by H. If the TPMS-member is balanced, then the operation α maps one branch of the family onto the other, in particular $v(H) = 1 - v(-H)$, $v(H = 0) = v_0 = 0.5$ and $A(H) = A(-H)$. For an amphiphilic monolayer of thickness δ in a ternary system, v can be identified with the hydrocarbon volume fraction (that is oil and amphiphilic tails), $1 - v$ with the water volume fraction (where we neglect the contributions of the amphiphilic heads), and $2A\delta$ with the amphiphile volume fraction. In the seminal work by Anderson, Davis, Nitsche and Sciven from 1990, the CMC-families were numerically constructed for P, D, I-WP, F-RD and C(P) using finite element methods [2]. In 1997, Grosse-Brauckmann numerically constructed the G-family in a similar way (using the software package *Surface Evolver*) [44]. For these families, the following data has been tabulated: volume fraction v as a function of scaled mean curvature H^* and scaled surface area A^* as a function of v. Rearrangement and interpolation with cubic splines provides smooth functions $H^*(v)$ and $A^*(v)$. As v is varied away from the value v_0 for the TPMS (= 0.5 for balanced structures), one has

$$H^*(v) = -\frac{(v - v_0)}{c} + \mathcal{O}\left((v - v_0)^2\right) \qquad (23)$$
$$A^*(v) = A_0 - \frac{(v - v_0)^2}{c} + \mathcal{O}\left((v - v_0)^3\right)$$

where the numerical value of c can be extracted from the cubic splines (compare Tab. 5). Note that the two relationships are not independent due to the relation $dA/dV = 2H$. They are related through c, whose values are well approximated

by the analogous values for the parallel surface companions to the TPMS, which can be derived as follows [98]: if δ denotes the perpendicular distance from the minimal to its parallel surface, to lowest order in δ the volume fraction v and the mean curvature H^*, averaged over the surface in the unit cell, are given by $v = v_0 + A^*\delta$ and $H^* = 2\pi\chi\delta/A^*$, respectively. Thus $H^* = 2\pi\chi(v - v_0)/{A^*}^2$ and $c = -{A^*}^2/2\pi\chi$ for the parallel surface case. The corresponding numbers are given in Tab. 5; except for C(P), the overall agreement with the numerical data for c for the CMC-surfaces is remarkably good.

Eq. (23) is a useful approximation for CMC-surfaces close to the TPMS, where they behave similar to parallel surfaces. However, as mean curvature grows, the numerical data starts to deviate from these approximations, changes in v and A^* become slower, and a turning point is reached, where v reaches an extremal value and starts to decrease again as a function of H. Beyond the turning point, the surfaces correspond to nearly spherical regions connected by small necks which resemble pieces of unduloids. Finally these necks disappear and each branch terminates in an assembly of sphere, which might be close-packed or self-intersecting. Fig. 9 shows the geometrical data for the families G, D, P, C(P), I-WP, F-RD as tabulated in the literature [2, 44]. We do not show the parts of the data beyond the turning point, as these correspond to surfaces whose structure is unphysical.

We now consider a ternary mixture of water, oil and amphiphile, where amphiphiles self-assemble into monolayers with spontaneous curvature c_0. In such a system, all relevant phases (micellar, hexagonal, lamellar, cubic bicontinuous) can be modeled as CMC-surfaces (spheres, cylinders, planes, triply periodic CMC-surfaces). This approach has first been used by Safran and coworkers [94, 95, 116], who in particular discussed the surfaces from the D-family. In our work [98], we extended this analysis to all families of interest, including the G-family, for which the relevant data has become available only recently and which features very prominently in experimental systems. A ternary mixture has two independent degrees of freedom for concentration, which we choose to be the hydrocarbon volume fraction v and the ratio w of amphiphile to hydrocarbon volume fraction. For the formulae given later it is in fact useful to modify the definition of w and to scale it with the dimensionless spontaneous curvature c_0: $w = \rho_A/vc_0\delta$. The analysis of Eq. (1) for CMC-surfaces is simplified considerably by the fact that as mean curvature H is constant, there is no difference between local and global curvature properties and the integral over the surface becomes trivial. We use a factor $2\kappa c_0^3$ to rewrite the free-energy density in the dimensionless form

$$f = \frac{A}{c_0 V}\left(\frac{H}{c_0} - 1\right)^2 - \frac{2\pi\chi r}{{c_0}^3 V} \ . \tag{24}$$

For phases with lamellar, cylindrical and spherical aggregates, this free-energy density can easily be expressed as a function of the concentration degrees of

freedom:

$$f_L(w,v) = wv, \tag{25}$$

$$f_C(w,v) = wv\left(\frac{w}{4}-1\right)^2, \tag{26}$$

$$f_S(w,v,r) = wv\left[\left(\frac{w}{3}-1\right)^2 - \frac{rw^2}{9}\right]\ . \tag{27}$$

Note that only f_S depends on r, since the other two structures have no Gaussian curvature. Since the aggregates are disconnected, the dependence on v is trivial. The phase boundaries $S-C$, $S-L$, $C-L$ and the emulsification failure are obtained from Eqs. (25), (26) and (27) to be $w = 24/(7-16r)$, $w = 6/(1-r)$, $w = 8$ and $w = 3/(r-1)$, respectively. For example, for $r = 0$ and increasing w, we find the phase sequence L - C - S - emulsification failure, which is typical for amphiphilic systems (for simplicity, we identify phase transitions with crossing points of the free-energy-density curves, and use the Maxwell construction only for the emulsification failure). In Fig. 4 one sees that experimentally the emulsification failure indeed occurs at constant w (straight line through water apex). For increasing r, the spherical phase becomes more favorable and finally suppresses the cylindrical phase.

The structures based on CMC-surfaces discussed here are very different from the lipid bilayer structures discussed in the preceding section: now only one monolayer is present, and one of the two labyrinths is filled with hydrocarbon. In the following, they are called *single structures*. It should be noted that for non-balanced structures, it makes a difference which of the two labyrinth is filled with hydrocarbon; for example, the I-WP-family generates two single structures, which we call I and WP. In ternary amphiphilic systems there also exists an analogue to the bilayer structures discussed before, which we call *double structures* and mark with an index I. Double structures have the same geometries like cubic bicontinuous phases in diblock copolymer systems. They can be considered to be TPMS-based bilayer structures where the inner part of the bilayer has been swollen with suitable solvent. Since each of the two monolayers has the same spontaneous curvature c_0, a double structure can be modeled as the combination of the two surfaces of a CMC-family with $H = c_0$ and $H = -c_0$. Since for not too large H these two CMC-surfaces essentially correspond to the shrinkage of one of the two separate labyrinths defined by the minimal surface member, the two interfaces of a double structure do not intersect. Note that in principle there exists another class of structures, that is double structures where oil and water (and therefore amphiphile orientation and mean curvature) have been reversed. However, since finite spontaneous curvature selects only phases with curvature towards one specific side, they are suppressed for energetic reasons by the lamellar phase.

In our work [98], we considered 8 different single structures, which exist for the volume intervals $[0.056, 0.944]$ for G, $[0.131, 0.869]$ for D, $[0.249, 0.751]$ for P, $[0.481, 0.519]$ for C(P), $[0.357, 0.857]$ for I, $[0.143, 0.643]$ for WP, $[0.439, 0.625]$ for F and $[0.375, 0.561]$ for RD. We also considered 6 double structures, which

exist for the volume intervals $[0.112, 1.0]$ for G_I, $[0.262, 1.0]$ for D_I, $[0.498, 1.0]$ for P_I, $[0.962, 1.0]$ for $C(P)_I$, $[0.624, 1.0]$ for I-WP_I and $[0.818, 1.0]$ for F-RD_I. Note that the gyroid structures cover the largest intervals in v for their respective class: there is no other structure which can incorporate so extreme volume fractions like the gyroid. Together with the 3 non-cubic phases treated above, we considered 17 different phases. Since the cubic phases consist of one connected aggregate, the scaling of the free energy density f with hydrocarbon volume fraction v will be non-trivial. For a given value of v, the mean curvature $H(v, a) = H^*(v)/a$ and the surface area $A(v, a) = A^*(v)a^2$ within a unit cell are determined by the curves plotted in Fig. 9. The amphiphile concentration $\rho_A = A(v, a)/a^3 = A^*(v)/a$ fixes a, so that $a = A^*(v)/\rho_A = A^*(v)/(wvc_0)$. From Eq. (24) we can then derive

$$f_{BC}(w, v, r) = wv\left[\Lambda(v)\ wv - 1\right]^2 + r\ \frac{(wv)^3}{\Gamma(v)^2} \tag{28}$$

where we have used the definition for the curvature index Λ and the topology index Γ from Eq. (7). Note that now the indices are v-dependent. For the single structures, f follows by combining using the data shown in Fig. 9 with the definitions in Eq. (7). For the double structures, the procedure is somehow more complicated. However, for balanced double structures, it becomes simple again, one then can use

$$\Lambda_I(v) = \Lambda(v/2)/2, \Gamma_I(v) = 2\Gamma(v/2), f_{BC,I}(w, v, r) = 2f_{BC}(w, \frac{v}{2}, r) \tag{29}$$

in Eq. (28).

For $r = 0$ (vanishing saddle splay modulus $\bar{\kappa}$), the analysis of cubic bicontinuous phase behavior becomes rather simple: in contrast to the case of the parallel surface model discussed in the last section, now the bending energy given in Eq. (28) can be completely relaxed, namely by satisfying $w(v) = 1/v\Lambda(v)$. This leads to lines of vanishing frustration in the Gibbs triangle. For the free-energy density of the micellar and hexagonal phases (Eq. (27) and Eq. (26), respectively), the lines of vanishing frustration follow as $w = 3$ and $w = 4$, respectively. All lines of vanishing frustration are plotted in Fig. 10a. Obviously for this case phase behavior is very complex and degenerated, since every structure considered has some region of stability around its line of vanishing frustration. This type of degeneracy caused by the bending energy has been discussed before [6] and leads to the conclusion that additional physical effects have to be operative, as it is not observed in experimental systems.

Using Eq. (23), a simple approximation can be derived for the lines of vanishing frustration of the cubic phases:

$$w = -cA_0/v_0(v - v_0), w_I = -4cA_0/(v - 1)\ . \tag{30}$$

Thus the minimal surface case corresponds to the stable solutions for $w \gg 1$ at $v = v_0$ and $v = 1$, respectively. For the balanced single structures and the double structures the hierarchy of the different phases within the band-like

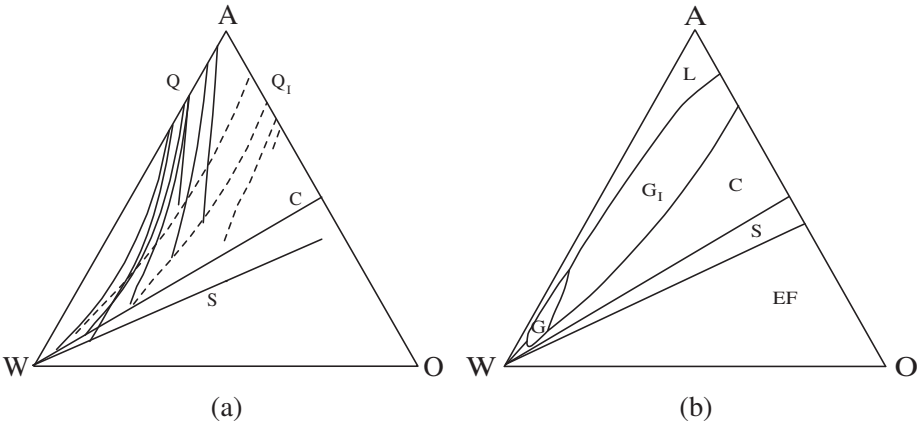

Figure 10: (a) Lines of vanishing frustration for $r = 0$. With increasing amphiphile concentration, the structures S - C- double cubic - single cubic are stable. (b) Phase behavior for $r = 1/15$. Now all cubic phases have been suppressed except the two gyroid phases. In (a) and (b), $c_0 = 1/6$, which corresponds to $H_2O/C_{14}/C_{12}E_5$ at $T = 20°C$.

region occupied by a certain structural type is thus determined by the values of cA_0. Using the approximation $c \approx -A^{*2}/2\pi\chi$ derived above, we find $cA^* \approx \Gamma^2$, where A^* and Γ correspond to the minimal surface members. Therefore the phase sequence is approximately determined by the topology index of the minimal-surface member of each family. In particular, for a given structural type we expect to find the sequence G - D - P as a function of either v or w.

For $r > 0$ (negative saddle splay modulus $\bar{\kappa}$), spheres become more favorable, cubic phases less favorable and cylinders and lamellae experience no change in free energy. Therefore the cubic phases will finally disappear, but our numerical analysis shows that cubic phases can persist up to $r = 0.2$, in contrast to earlier work, which predicted $r = 0.1$ [116]. The reason for this becomes clear in Fig. 10b where we show the full phase diagram for $r = 1/15 = 0.07$: the only cubic phases stable here are the two gyroid structures, which have not been considered before. There are two main reasons for their outstanding performance: Eq. (28) shows that their large values for the topology index Γ reduces the energetic penalty caused by r, and since they can accommodate extreme volume fractions, they can compete with other structures at all relevant concentrations. By comparing the theoretical phase diagram from Fig. 10 with the experimental one from Fig. 5, we conclude that the experimental system should correspond to a rather large value of r. Earlier work moreover suggests that incorporation of thermal fluctuations would favor micellar phases near the water-amphiphilic side and lamellar phases near the water apex [101]. Such a modification is expected to considerably improve the agreement between the two phase diagrams.

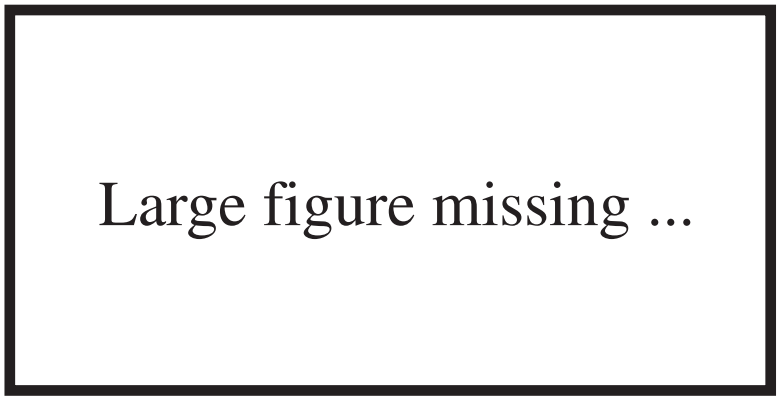

Figure 11: Freeze-fracture microscopy picture of a balanced microemulsion phase. From Ref. [52].

6 Random surfaces

6.1 Microemulsion and Sponge Phases

When κ/k_BT, the bending rigidity in thermal units, becomes sufficiently low (that is temperature T sufficiently high), bicontinuous structures can now longer maintain their long-range crystalline order and melt into a disordered phase, which is characterized by an exponential decay of correlations in the interfacial positions. Such phases have been observed experimentally for a long time in many binary and ternary amphiphilic systems. *Microemulsions* are macroscopically homogeneous and optically isotropic mixtures of oil, water and amphiphiles. On a mesoscopic scale, they consist of two multiply connected and intertwined networks of oil- and water-channels, which are separated by an amphiphilic monolayers. Free-fracture microscopy, where the sample is quickly frozen, cut, and then studied with an electron microscope, reveals the intriguing structure of this phase [52], see Fig. 11. A similar phase, the *sponge phase*, appears in binary systems of water and amphiphile, where now the two labyrinths are occupied by water, which are separated by an amphiphilic bilayer. The pictures obtained by free-fracture microscopy [107] are even more suggestive in this case, because the sample has a preference to break along the bilayer mid-surface, so that the three-dimensional structure of the membrane becomes visible. An example is shown in Fig. 12, which clearly shows the saddle-like geometry of the amphiphile film. Therefore, the intuitive picture of microemulsion and sponge phases as fluid versions of bicontinuous cubic phases is strongly supported by these experiments.

These phases have been investigated experimentally in considerable detail over many years. In particular, their phase behavior and scattering intensities have been studied carefully. A theoretical understanding of the statistical

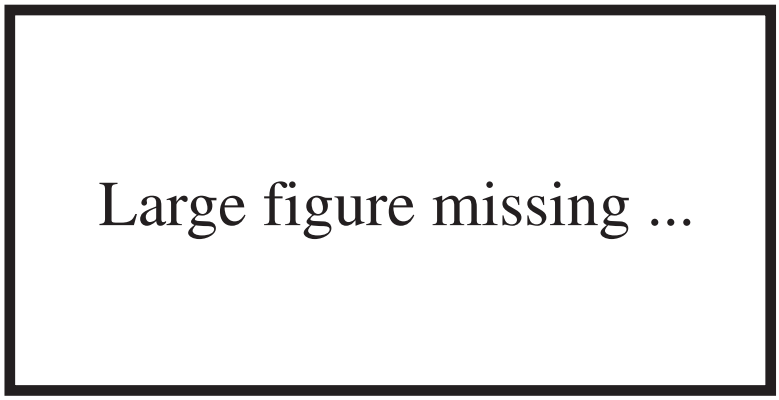

Figure 12: Freeze-fracture microscopy picture of a sponge phase. From Ref. [107].

mechanics of membranes, however, is only beginning to emerge in recent years [75, 40, 78, 18, 35]. This is no surprise, since the statistical mechanics of a surface, which can not only change its shape, but also its topology in all possible ways, is extremely complicated. In principle, a partition function of the form

$$Z = \sum_{topologies} \int' \mathcal{D}\mathbf{R}(\tau) \exp\{\mathcal{H}[\mathbf{R}(\tau)]/k_B T\} \tag{31}$$

has to be calculated, where $\mathcal{D}\mathbf{R}(\tau)$ denotes an integration over all possible shapes with parametrization $\mathbf{R}(\tau)$ of the surface at fixed topology, where τ is a two-dimensional coordinate system on the surface. However, this integral cannot be just over all possible parametrization $\mathbf{R}(\tau)$ of a surface of fixed topology, but has to be restricted to those parametrizations, which lead to physically different shapes in the embedding space; this is indicated by the prime. Finally, the contributions off all different topologies have to be summed over. It is clear that this problem is sufficiently complex that no exact solution will be found anytime soon. Therefore, approximations have to be made in order to get some insight into the behavior of these phases.

6.2 Gaussian random fields

A very useful approach is to describe the interfaces as isosurfaces of *Gaussian random fields* (GRF). This corresponds to a Ginzburg-Landau model as discussed in Sec. 2.2, in which the free-energy functional is taken to be quadratic in the scalar field $\Phi(\mathbf{r})$. This Gibbs distribution is homogeneous and isotropic, and all the functional integrals are Gaussian and can be performed exactly. In fact, there is a considerable mathematical literature on the isosurfaces of GRF, see e.g. the book by Adler [1]. In order to comply with the conventions of this

field, we now make two changes to our notation. In the following, area content is denoted by S (rather than by A) and amphiphilic (hydrocarbon) volume fraction by Ψ (rather than by v).

The amphiphilic monolayers in microemulsions have been modelled as level surfaces of GRF by Berk [4, 5], Teubner [112], Pieruschka and Marcelja [81], and Pieruschka and Safran [82, 83]. Here the starting point is a Gaussian free-energy functional of the general form

$$\mathcal{H}_0[\phi] = \frac{1}{2} \int d^3q \, \nu(\mathbf{q})^{-1} \Phi(\mathbf{q}) \Phi(-\mathbf{q}) \ . \tag{32}$$

The average geometry of the $\Phi(\mathbf{q}) = \alpha$ level surfaces can be calculated for arbitrary spectral density $\nu(\mathbf{q})$. For the surface density, S/V, the mean curvature H, the Gaussian curvature K, and the mean curvature squared H^2, the following averages are obtained [112]:

$$\frac{S}{V} = \frac{2}{\pi} \exp\left[-\frac{\alpha^2}{2}\right] \sqrt{\frac{1}{3}\langle q^2 \rangle} \ , \tag{33}$$

$$\langle K \rangle = -\frac{1}{6} \langle q^2 \rangle (1 - \alpha^2) \ , \tag{34}$$

$$\langle H \rangle = \frac{1}{2} \alpha \sqrt{\frac{\pi}{6} \langle q^2 \rangle} \ , \tag{35}$$

$$\langle H^2 \rangle = \langle K \rangle + \frac{1}{5} \frac{\langle q^4 \rangle}{\langle q^2 \rangle} \tag{36}$$

where

$$\langle q^n \rangle = \int \frac{d^3q}{(2\pi)^3} q^n \nu(\mathbf{q}) \ . \tag{37}$$

The value α of the level cut can be used to describe the preferred curvature of the membrane, as well as the volume fractions of oil and water. Since $\langle H \rangle$ is a linear function of α, compare Eq. (35), this parameter is proportional to the spontaneous curvature c_0. In particular, for $\alpha = 0$ the mean curvature of the surface vanishes; this applies to a balanced system, where $c_0 = 0$.

For balanced systems, it follows from Eqs. (33,34) that the topology index $\Gamma = \sqrt{8}/\pi = 0.9003$ (compare Eq. (7)). This value is only slightly larger than the ones for cubic bicontinuous phases (compare Tab. 1), since the balanced random sponge features only few disconnected parts (note that Γ doubles when the structure is duplicated). For small curvatures (that is small α), one can use Eqs. (33,34,35) to derive a relationship between topology index Γ and curvature index Λ which is independent of spectral density $\nu(\mathbf{q})$ and α:

$$\Gamma = \frac{\sqrt{8}}{\pi} \left(1 + \frac{2^8}{\pi^6} \Lambda^4 + \dots \right) \ . \tag{38}$$

When the curvature index Λ increases since the sponge's interfaces gain curvature, the topology index increases, too, since disconnected parts proliferate.

The GRF-approach is most predictive when the Gaussian model of random interfaces is related to the statistical mechanics of membranes by a variational approximation [82, 83]. In this case, the spectral density $\nu(\mathbf{q})$ in the functional (32) is determined by the requirement that the $\phi(\mathbf{r}) = 0$ level surfaces mimic the behavior of interfaces controlled by the curvature Hamiltonian (1) as close as possible. The usual variational approach employs the Feynman-Bogoljubov inequality,

$$F \leq F_0 + \langle \mathcal{H} - \mathcal{H}_0 \rangle_0 \tag{39}$$

where $\mathcal{H}$ and F are the Hamiltonian and the free energy of the system of interest, respectively, and $\mathcal{H}_0$ and F_0 the same quantities of the reference system. In this way, an upper bound for the true free energy is obtained. This is more complicated in the case of random surfaces, because the GRF-Hamiltonian is defined everywhere in space, while the curvature Hamiltonian is only defined on the level surface. Therefore, the curvature energy does not restrict fluctuations of the field $\Phi(\mathbf{r})$ away from the level surface. In order to suppress such fluctuations, one usually makes the *mean-spherical approximation*, that is the constraint $\langle \Phi(\mathbf{r})^2 \rangle = 1$ is introduced.

With this variational approach, Pieruschka and Safran [82] have been able to derive the following form for the spectral density

$$\nu(\mathbf{q}) = \frac{a}{q^4 + bq^2 + c} \tag{40}$$

and to relate the parameters a, b and c to the curvature elastic moduli κ and $\bar{\kappa}$ and the surface density S/V. The first interesting result is that the spectral density is found to be *independent* of $\bar{\kappa}$. Exact expressions for the parameters can be found in Ref. [22]. To leading order in k_BT/κ, the parameters simplify to

$$a = \frac{15\pi^2}{16} \frac{k_BT}{\kappa} \frac{S}{V} , \tag{41}$$

$$b = \frac{3}{2}\pi^2 \left(\frac{S}{V}\right)^2 , \tag{42}$$

$$c = \left(\frac{3\pi^2}{4}\right)^2 \left(\frac{S}{V}\right)^4 . \tag{43}$$

The spectral density (40) is equivalent to the scattering intensity in bulk contrast. Its Fourier transform yields the correlation function

$$\langle \Phi(\mathbf{r})\Phi(\mathbf{r}') \rangle = \int d^3q \; e^{i\mathbf{q}\cdot(\mathbf{r}-\mathbf{r}')} \nu(\mathbf{q}) = \frac{A}{r} \; \exp[-r/\xi] \; \sin(kr) \tag{44}$$

where the second equality holds for $|b| < 2\sqrt{c}$. Thus, the correlation function is characterized by two length scales, the correlation length ξ and the typical domain size $d = 2\pi/k$ of the oil- of water channels, which are obtained from

Eqs. (40) and (44) to be [113]

$$\xi^{-1} = \frac{1}{2}\sqrt{2\sqrt{c}+b}\,, \tag{45}$$

$$k = \frac{1}{2}\sqrt{2\sqrt{c}-b}\,. \tag{46}$$

With the results (41), (42) and (43), the asymptotic behavior for small k_BT/κ of the dimensionless product $k\xi$ is found to be

$$k\xi = \frac{64}{5\sqrt{3}}\ \frac{\kappa}{k_BT}\ . \tag{47}$$

The free energy of the sponge phase can also be calculated from the GRF approach. To leading order in an expansion in k_BT/κ, the free-energy density $f = F/V$ is found to be [83]

$$f = \frac{\pi^2}{40}[2\kappa - 5\bar{\kappa}]\left(\frac{S}{V}\right)^3 - \frac{k_BT}{12}\ln\left(\delta\frac{S}{V}\right)\ . \tag{48}$$

This implies that for small membrane volume fractions $\Psi = \delta S/V$ (where again δ is the thickness of the amphiphilic interface), the entropic term dominates over the energy term, and that the sponge phase becomes unstable in this regime.

We want to end this section with a short discussion of the reliability of the predictions of the GRF model as a variational approximation for membrane ensembles. The weak point of this approach is that it is not clear whether the calculated entropy is actually equivalent to the physical conformational entropy of the membranes [74]. The main problem is that the curvature energy only controls the shape of the $\Phi(\mathbf{r}) = 0$ level surface, while the values of the scalar field Φ at all other points in space are not affected by it. The fluctuations of Φ in these oil- and water-regions are mainly determined by the mean-spherical constraint $\langle\Phi^2(\mathbf{r})\rangle = 1$. Obviously, an appreciable contribution to the total entropy arises from the fluctuations of Φ these 'bulk' regions. This would not affect the predictions of the model as long as the 'bulk' contributions were independent of the interface positions. Unfortunately, there is no argument so far that this is indeed the case.

6.3 Phase behavior of random surfaces

From here on we consider only the case of vanishing spontaneous curvature, $c_0 = 0$, that is balanced microemulsions and sponge phases. Then the phase behavior is controlled by the bending rigidity κ, the saddle-splay modulus $\bar{\kappa}$, the density of membrane area per volume, S/V, and a microscopic cutoff δ, which can be identified with the thickness of the amphiphilic interface. It is very important to realize that for vanishing spontaneous curvature, phase transition as a function of the amphiphile volume fraction cannot be understood on the basis of the curvature energy alone — i.e. without considering the effect of thermal fluctuations [85]. The reason is that the curvature Hamiltonian is

conformally invariant in three spatial dimensions, which implies in particular that it is invariant under a simultaneous rescaling of all length scales. Since the curvature energy is scale invariant, the energy *density* scales as the third power of an inverse length, i.e. as $(S/V)^3$. Therefore, the curvature energy of any given structure — spherical, cylindrical, lamellar, cubic, or random — scales in exactly the same way with decreasing amphiphile volume fraction, and their relative order is maintained. Therefore, thermal fluctuations are crucial for these phase transitions.

It has been suggested by several authors [93, 9, 73, 28] that the free energy of the sponge phase can be obtained by integrating out the membrane fluctuations on scales less than the typical domain size. This integration over small-scale fluctuations leads to renormalized, scale-dependent curvature moduli $\kappa_R(l)$ and $\bar{\kappa}_R(l)$ as given by Eqs. (4) and (5), respectively, with $l/\delta = \Psi^{-1}$, where Ψ is the membrane volume fraction. This implies that the curvature Hamiltonian (2) has to be replaced by

$$F = \int dA \left\{ \frac{1}{2}\kappa_{+,R}(\Psi^{-1})(k_1+k_2)^2 + \frac{1}{2}\kappa_{-,R}(\Psi^{-1})(k_1-k_2)^2 \right\} \qquad (49)$$

with

$$\kappa_{+,R}(\Psi^{-1}) = \kappa_+ + \frac{k_B T}{3\pi} \ln \Psi \ , \qquad (50)$$

$$\kappa_{-,R}(\Psi^{-1}) = \kappa_- + \frac{5 k_B T}{12\pi} \ln \Psi \ . \qquad (51)$$

The stability arguments used in Sec. 2.1 imply that $\kappa_{+,R}$ and $\kappa_{-,R}$ have to be positive for the free energy (49) to be stable against collapse of the structure to molecular scales. Therefore, there are instabilities at $\kappa_{+,R}(\Psi^{-1}) = 0$ and $\kappa_{-,R}(\Psi^{-1}) = 0$. The latter instability can be identified with the emulsification failure of the sponge phase, so that the phase boundary is predicted to occur at [73]

$$\ln \Psi = \frac{6\pi}{5} \ \frac{\bar{\kappa}}{k_B T} \ . \qquad (52)$$

This result can be understood intuitively as follows. For sufficiently large membrane volume fraction, both $\kappa_{+,R}$ and $\kappa_{-,R}$ are positive. Therefore, the system tries to minimize $(k_1+k_2)^2$ and $(k_1-k_2)^2$. This can be achieved by decreasing both k_1 and k_2, i.e. by swelling a given structure as much as possible — the lamellar or sponge phase is stable at this value of Ψ. On the other hand, as soon as $\kappa_{+,R}$ or $\kappa_{-,R}$ become negative at some small value of Ψ, the free energy can be reduced by collapsing the structure. With decreasing length, however, $\kappa_{+,R}$ and $\kappa_{-,R}$ increase and finally become positive. Therefore, the collapse stops at a length scale which is exactly the length scale determined by Eq. (52).

It is worth mentioning that a similar result follows from the calculation of the shapes and free energies of passages in lamellar phases [31]. Passages are catenoid-like connections between adjacent lamellae which proliferate close to

phase transitions to disordered bicontinuous phases. From a detailed calculation, which takes into account the Gaussian membrane fluctuations, the density, ρ, of passages per unit base area of the stack can be obtained to be

$$\rho = \frac{A_0(\kappa/k_BT)}{\delta^2} \left(\frac{d}{\delta}\right)^{4/3} \exp[4\pi\bar{\kappa}/k_BT] \tag{53}$$

Here, $A_0(\kappa/k_BT)$ is a function which has to be calculated numerically; it is predicted to increase monotonically with decreasing κ/k_BT in Ref. [31]. Therefore, the density of passages increases with increasing lamellar spacing $d/\delta = \Psi^{-1}$. When the average distance between passages shrinks to the average membrane separation, a transition to the sponge phase can be expected to occur. This happens at

$$\frac{10}{3} \ln \Psi/\Psi^* = 4\pi \frac{\bar{\kappa}}{k_BT} \tag{54}$$

where Ψ^* is a function of κ/k_BT. Equations (52) and (54) agree perfectly.

The consideration of the renormalization of κ and $\bar{\kappa}$ implies that the free-energy density, f, of the sponge phase should behave as [89, 87, 90]

$$f = (A + B \ln \Psi)\Psi^3 \ . \tag{55}$$

As explained above, the overall scaling with Ψ^3 derives from the conformal invariance of the curvature energy. A represents the bending energy without thermal fluctuations, and is a linear function of both κ and $\bar{\kappa}$. B represents the logarithmic corrections from the renormalization and is a linear function of temperature. Both A and B depend on the detailed geometrical structure of the sponge phase, and thus cannot be obtained from simple scaling arguments. It is important to note that the functional dependence of the free energy (55), which is based on the renormalization of the curvature elastic moduli due to *small-scale* membrane fluctuations, does not agree with the free energy (48) of the Gaussian random field model, which includes the topological entropy of a disordered bicontinuous phase.

6.4 Monte Carlo simulations of triangulated surfaces

In order to go beyond the approximations discussed in Secs. 6.2 and 6.3, discretized surface models can be investigated by Monte Carlo simulations [35, 34, 36, 37]. Surface triangulations provide the best way of discretizing a surface as uniformly as possible. The model consists of vertices, which are connected by bonds in such a way that the bonds form a triangular network. Several Hamiltonians have been suggested for triangulated surfaces, such that their shapes and fluctuations are governed in the continuum limit by the curvature energy from Eq. (1) [35]. Two examples are Gaussian-spring models, in which neighboring vertices — the vertices connected by bonds — interact with harmonic spring potentials, and tether-and-bead models, in which the interaction $V(r)$ between

neighboring vertices is defined the potential

$$V(r) = \begin{cases} \infty & 0 \le r < \sigma_0 \\ 0 \quad \text{for} & \sigma_0 < r < \ell_0 \\ \infty & \ell_0 < r \end{cases} \tag{56}$$

where σ_0 is the hard-core diameter of the beads, and ℓ_0 is the tether length. For tether lengths $\ell_0 < \sqrt{3}\sigma_0$, the network is self-avoiding, because a bead of some distant part of the membrane does not fit through the hole between the three beads of a triangle, even for maximally stretched tethers.

A Monte Carlo simulation of sponge phases requires three types of Monte Carlo moves [36]. The first step is to displace selected beads by a random vector chosen uniformly in the cube $[-s, s]^3$. Here, s is determined by the criterion that roughly 50% of trial moves is accepted according to the Boltzmann weight. The second step is to vary the connectivity of the bond network, in order to allow for diffusion and fluidity of the membrane. This dynamic triangulation is performed for any two adjacent triangles. The bond which forms the common edge of the two triangles is cut, and a new bond is inserted, which connects the two previously unconnected beads. The bond can only be cut if every bead retains bonds to at least three other beads. This procedure guarantees that the network remains two-dimensionally connected, no holes open up in the network, and the topology of the network does not change. Finally, the third step is to change the topology of the surface. This is done by removing two nearby triangles from the surface, and by connecting the corresponding vertices by a prism of six new triangles. Of course, the inverse step is also possible, with a passage six triangles being removed, and two new triangles inserted to close the surfaces. The acceptance of both the bond-flip and topology-change moves is determined by the Boltzmann weight and is therefore controlled by the curvature energy. We want to mention parenthetically that some care has to be taken to find a good discretization of the bending energy [33].

A typical configuration of a triangulated surface in a cubic box with parameters κ, $\bar{\kappa}$ and Ψ chosen in the stability region of the microemulsion or sponge phase is shown in Fig. 13. This configuration nicely demonstrates the bicontinuous structure of balanced microemulsions and sponge phases. The saddle-like geometry of the membrane can also be easily seen. Finally, the figure shows that *locally* the structure of the sponge phase strongly resembles the cubic phases discussed above. Therefore, a sponge phase should indeed be considered as the molten state of the crystalline cubic phase.

A more quantitative comparison with the theoretical approaches of Secs. 6.2 and 6.3 above can be made by determining the phase diagram of the randomly-triangulated surface model, and by calculating the osmotic pressure, p, in the simulations as a function of the membrane volume fraction Ψ. From Eq. (55), we obtain

$$\begin{aligned} p\delta^3/k_BT &\equiv \frac{1}{k_BT}[\Psi \partial f/\partial \Psi - f] \\ &= [(2A + B) + 2B \ln \Psi]\, \Psi^3 \end{aligned} \tag{57}$$

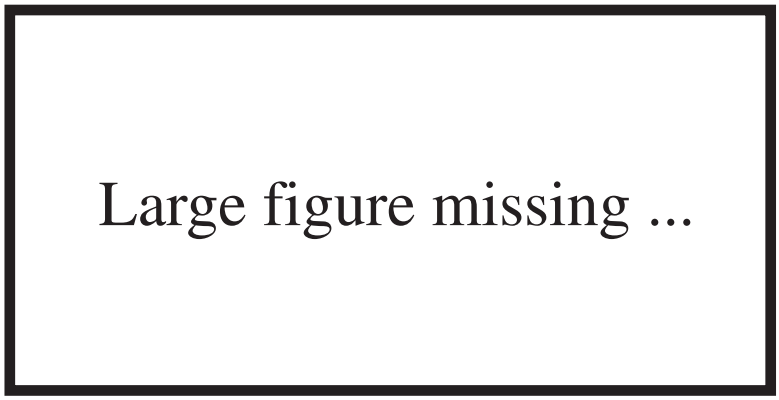

Figure 13: A typical membrane configuration in a sponge phase for bending rigidity $\kappa/k_BT \simeq 1.6$. The two sides of the membrane are shaded differently in order to emphasize the bicontinuous structure of this phase. From Ref. [36].

i.e. the same functional dependence as the free-energy density itself. This dependence of the osmotic pressure is indeed nicely confirmed by the simulation data [36]. The simulations therefore provide strong evidence for the renormalization of the elastic moduli of the curvature model and for the dependence (55) of the free energy on the membrane volume fraction.

The phase diagram for fixed bending rigidity κ is shown as a function of $\bar{\kappa}$ and Ψ in Fig. 14. The simulation data are compared with the prediction (52) for the phase boundary. Since the slopes of the phase boundaries in this logarithmic plot agree very well, not only the exponential dependence of the membrane volume fraction at the transition on the saddle splay modulus is confirmed, but also the value of the universal prefactor in Eq. (52) is strongly supported.

6.5 Comparison with experiments

Experimentally, phase diagrams and scattering intensities have been studied systematically for many different surfactant molecules. Qualitatively, the agreement with the theoretical approaches is very reasonable. For example, the scattering curve in bulk contrast shows a peak at non-zero wave vector in the microemulsion phase, which moves out and decreases in height with increasing surfactant concentration. A quantitative comparison, however, is much more difficult. We want to discuss here three different classes of experiments, where a such a quantitative comparison has been made.

The first type of experiments are scattering studies in bulk and film contrast. In bulk contrast, the scattering intensity $S_{ww}(\mathbf{q})$ is proportional to the spectral density $\nu(\mathbf{q})$ of the Gaussian random field model, compare Eq. (40), for wave vectors q which are not much larger than the characteristic wave vector k of

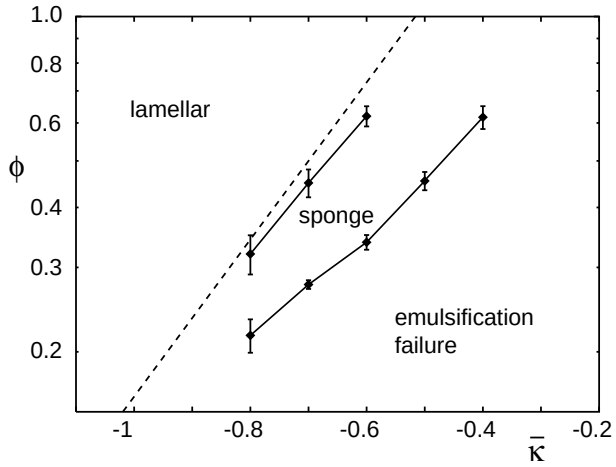

Figure 14: The phase diagram as a function of membrane volume fraction Φ and saddle-splay modulus $\bar{\kappa}$, for bending rigidity $\kappa/k_BT \simeq 1.6$. Note the logarithmic scale of the abscissa. The dashed line shows the theoretical prediction (52). From Ref. [36].

the domain structure, compare Eq. (46). The functional dependence of Eq. (40) describes the scattering data in this regime very well, as was first noted by Teubner and Strey [113], who derived this result on the basis of a Ginzburg-Landau model, very similar to that introduced in Sec. 2.2. We want to mention parenthetically, that for wave vectors $k \ll q \ll 1/\delta$, the intensity is dominated by the scattering from sharp, planar interfaces; in this limit, the famous Porod law [84, 112] predicts $I(q) \sim (S/V)q^{-4}$.

In the limit of wave vector $q \to 0$, the scattering intensity in film contrast is given by [87]

$$I(q \to 0) \sim \Psi \left(\frac{\partial p}{\partial \Psi} \right)^{-1} \tag{58}$$

where p is the osmotic pressure of Eq. (57). For the free energy (55), this implies

$$[\Psi I(q \to 0)]^{-1} \sim const + \ln \Psi \tag{59}$$

Such a behavior has indeed be observed experimentally in Ref. [87]. However, this result has been questioned by Daicic et al. [14, 13]. This has lead to a intensive debate, with arguments against [15, 16] and in favor [91, 86] of the existence of a logarithmic renormalization of elastic moduli in the sponge phase.

In a second type of experiment, information about the average geometry of the surfactant film can be extracted from the scattering intensity in the regime $k < q \ll 1/\delta$. This information is contained in the corrections to the asymptotic $1/q^4$ law for smaller values of the wave vector [111]. Experimentally, the average

Gaussian curvature is found to be [11]

$$(V/S)^2\langle K\rangle = 1.25 \pm 0.10 \tag{60}$$

which is in excellent agreement with the Gaussian random field result $(V/S)^2\langle K\rangle = 1/\Gamma^2 = -\pi^2/8 = 1.23$ and simulations of the Φ^6-Ginzburg-Landau model [32, 30].

The third type of experiment concerns the phase behavior of mixtures of water and non-ionic surfactant as a function of temperature and surfactant concentration. As mentioned in Sec. 4, the saddle-splay modulus $\bar{\kappa}$ is a linear function of temperature in this case. Therefore, the concentrations at the phase boundaries of the lamellar and the sponge phase are expected from Eq. (52) to depend exponentially on temperature. A logarithmic plot of the phase diagram of $C_{12}E_5$ in water [109], compare Fig. 4, is indeed consistent with this expectation.

The most detailed information about both the scattering intensities and phase behavior in these systems has been obtained very recently in ternary amphiphilic systems of water, oil and non-ionic surfactant C_iE_j, to which small traces of an amphiphilic block copolymer has been added [53, 21, 22, 29, 38]. The results obtained in this system provide further, strong evidence for the existence of a logarithmic renormalization of κ and $\bar{\kappa}$ in microemulsions and sponge phases.

7 Summary and outlook

In this contribution we discussed the geometrical properties of surfaces which can be used as structural models for cubic bicontinuous phases in amphiphilic systems: triply periodic minimal surfaces, their parallel surfaces and constant mean curvature companions, and bicontinuous random surfaces. For each class of surfaces, we showed how the geometrical properties translate into physical properties of bicontinuous phases in amphiphilic systems in the framework of an interfacial description. The surprising success of this approach relates to the fact that in amphiphilic systems, the solvent has little physical properties by itself and the free energy is essentially determined by the interfaces. Although there are several physical effects which have been neglected in our treatment of amphiphilic systems, including van der Waals and electrostatic interactions, it can be concluded that the most essential aspects of phase behavior are now well understood in terms of the properties of the underlying geometries.

During the last years, the interest in bicontinuous phases has increased due to some promising applications in the nano- and biosciences. For example, amphiphilic self-assembly has been used to synthesize *mesoporous systems* [58], that is porous material with amorphous walls (usually silica-based) and pore sizes on the nanometer scale. As a matter of fact, the combination of amphiphilic self-assembly and crystallization also seems to be a basic aspect of biomineralization [70], and there are many algae whose mineral skeletons look similar to cubic bicontinuous phases [51]. There is also a large effort underway to

synthesize bicontinuous structures from graphitic material (*Schwarzites*), which offers the advantage of atomically smooth walls [69]. Porous material on the nanometer scale is not only interesting for its structural properties (for example use as sieves or catalysts), but also for its electronic properties (for example use as photonic bandgap material).

In the biosciences, two recent developments involved cubic bicontinuous phases. It was found that the gyroid phase in the monoolein-water system provides a functional environment for the crystallization of integral membrane proteins like bacteriorhodopsin [77, 66]. Membrane proteins are notoriously difficult to crystallize in a three-dimensional array, which however is necessary for structure determination by X-ray scattering. And an extensive analysis of transmission electron micrographs of many biological specimen has shown that cubic bicontinuous structures are locally formed in several regions of the cells [61, 19], including endoplasmatic reticulum, Golgi apparatus and mitochondria. These are extended lipid bilayer systems in the cell which carry a protein machinery responsible for processing and packaging material inside the cell. In fact it is easy to imagine that biological cells regulate their lipid composition and therefore their spontaneous curvature as to achieve geometries favorable for the task at hand. In general, cubic bicontinuous phases seem to be ideal space partitioners if a large amount of active surface area is needed while simultaneously providing good access for incoming and outgoing material through the space away from the interface.

What problems are left regarding the subjects of this article ? From the viewpoint of mathematics, there are two interesting aspects. On the one hand, the physical motivation leads to certain variational problems for which little is known about the corresponding solutions. One example is the energy functional $\int dA(H - c_0)^2$ with a volume constraint; in principle this problem was subject of Sec. 5, but in lack of adequate mathematical knowledge (this problem has been treated for vesicles [104], but not for bicontinuous structures), we used CMC-surfaces as structural models. On the other hand, some classes of surfaces are well investigated, but still representations are missing which could be used in physical modelling. Therefore additional progress in regard to Weierstrass representations for TPMS, Weierstrass-like representations for their CMC-companions, and other (numerical) representations would be most welcome. With a larger repertoire of representations, it should also become easier to treat non-local effects like van der Waals and electrostatic interactions; here integral geometry might be helpful in reducing the dimensions of the corresponding integrals, and sophisticated summation techniques are needed to account for the infinite extension of the bulk phases.

From the viewpoint of material sciences, it seems worth to study the role of boundaries and inclusions. The term *boundaries* includes grain boundaries between different, yet adjacent phases, for example between a hexagonal and a gyroid phase; until now, this problem has been investigated only for simple geometries. It also includes the boundary to an external surface (which might even be curved or chemically structured) and free boundaries. For example, it has been recently observed experimentally that the bicontinuous cubic phase

in the binary system water - $C_{12}E_6$ is the only known material system which shows crystal faces with high Miller indices (*devil's staircase*) [80]. The term *inclusions* includes several object of biological and technological relevance, in particular integral membrane proteins, polymers anchored in the membrane and (functionalized) nanoparticles. In all of these cases, the framework described here should provide a good starting point for future research, which has to bridge the gap between the mathematical knowledge on the geometrical properties and the physics knowledge of the material basis of these fascinating structures.

8 WWW resources

Here we list some internet addresses which relate to the subject of this contribution:

- `http://www-sfb288.math.tu-berlin.de/~konrad/`:
  Homepage of Konrad Polthier, one of the pioneers for numerical representations and visualizations of minimal surfaces.
- `http://people.math.uni-bonn.de/kgb/`:
  Homepage of Karsten Grosse-Brauckmann, a mathematician working on CMC-surfaces, in particular on the G-family.
- `http://www.susqu.edu/facstaff/b/brakke/evolver/`:
  The *Surface Evolver* is a public domain software package written by Ken Brakke for the propagation of triangulated surfaces. In particular, Ken Brakke shows many examples of TPMS obtained with the *Surface Evolver*.
- `http://www.msri.org/publications/sgp/SGP/indexc.html`:
  The Scientific Graphics Project offers stunning visualizations of minimal and CMC-surfaces, obtained mostly in the framework of Weierstrass representations.
- `http://www.gang.umass.edu/`:
  The Center for Geometry, Analysis, Numerics and Graphics (GANG), where a lot of work on CMC-surfaces takes place.
- `http://www.mpikg-golm.mpg.de/th/people/schwarz/`:
  More information on the work described here, including color pictures of all structures investigated and (improved) nodal approximations.

References

[1] Adler, R. J., ed. (1981): *The Geometry of Random Fields* (Wiley, Chichester)

[2] Anderson, D. M., H. T. Davis, L. E. Scriven, J. C. C. Nitsche (1990): 'Periodic surfaces of prescribed mean curvature', *Adv. Chem. Phys.* **77**, pp. 337–397

[3] Anderson, D. M., S. M. Gruner, S. Leibler (1988): 'Geometrical aspects of the frustration in the cubic phases of lyotropic liquid crystals', *Proc. Natl. Acad. Sci. USA* **85**, pp. 5364–5368

[4] Berk, N. F. (1987): 'Scattering properties of a model bicontinuous structure with a well defined length scale', *Phys. Rev. Lett.* **58**, p. 2718

[5] Berk, N. F. (1991): 'Scattering properties of the leveled-wave model of random morphologies', *Phys. Rev. A* **44**, p. 5069

[6] Bruinsma, R. (1992): 'Elasticity and excitations of minimal crystals', *J. Phys. II France* **2**, pp. 425–451

[7] Cai, W., T. C. Lubensky, P. Nelson, T. Powers (1994): 'Measure factors, tension and correlations of fluid membranes', *J. Phys. II France* **4**, pp. 931–949

[8] Canham, P. B. (1970): 'The minimum energy of bending as a possible explanation of the biconcave shape of the human red blood cell', *J. Theor. Biol.* **26**, p. 61

[9] Cates, M. E., D. Roux, D. Andelman, S. T. Milner, S. A. Safran (1988): 'Random surface model for the l_3-phase of dilute surfactant solutions', *Europhys. Lett.* **5**, p. 733

[10] Charvolin, J., J. F. Sadoc (1990): 'Structures built by amphiphiles and frustrated fluid films', *J. Phys. (Paris) Colloq.* **51**, pp. 83–96

[11] Chen, S.-H., D. D. Lee, K. Kimishima, H. Jinnai, T. Hashimoto (1996): 'Measurement of the Gaussian curvature of the surfactant film in an isometric bicontinuous one-phase microemulsion', *Phys. Rev. E* **54**, pp. 6526–6531

[12] Cvijovic, D., J. Klinowski (1994): 'The computation of the triply periodic I-WP minimal surface', *Chem. Phys. Lett.* **226**, pp. 93–99

[13] Daicic, J., U. Olsson, H. Wennerström, G. Jerke, P. Schurtenberger (1995): 'Light scattering from the L_3 (sponge) phase: Evidence against logarithmic corrections to ideal scaling', *Phys. Rev. E* **52**, pp. 3266–3269

[14] Daicic, J., U. Olsson, H. Wennerström, G. Jerke, P. Schurtenberger (1995): 'Thermodynamics of the L_3 (sponge) phase in the flexible surface model', *J. Phys. II France* **5**, pp. 199–215

[15] Daicic, J., U. Olsson, H. Wennerström, G. Jerke, P. Schurtenberger (1996): 'Reply to "comment on 'thermodynamics of the L_3 (sponge) phase in the flexible surface model' "', *J. Phys. II France* **6**, pp. 95–96

[16] Daicic, J., U. Olsson, H. Wennerström, G. Jerke, P. Schurtenberger (1997): 'Reply to "comment on 'light scattering from the L_3 (sponge) phase: Evidence against logarithmic corrections to ideal scaling' "', *Phys. Rev. E* **56**, pp. 1278–1279

[17] David, F. (1989): 'Geometry and field theory of random surfaces and membranes', in Nelson, D., T. Piran, S. Weinberg, eds., 'Statistical Mechanics of Membranes and Surfaces', (World Scientific, Singapore), pp. 157–223

[18] David, F., P. Ginsparg, J. Zinn-Justin, eds. (1996): *Fluctuating geometries in statistical mechanics and field theory* (Elsevier, Amsterdam)

[19] Deng, Y., M. Marko, K. F. Buttle, A. Leith, M. Mieczkowski, C. A. Mannella (1999): 'Cubic membrane structure in amoeba (chaos carolinensis) mitochondria determined by electron microscopic tomography', *J. Struct. Biol.* **127**, pp. 231–239

[20] Düsing, P. M., R. H. Templer, J. M. Seddon (1997): 'Quantifying packing frustration energy in inverse lyotropic mesophases', *Langmuir* **13**, pp. 351–359

[21] Endo, H., J. Allgaier, G. Gompper, B. Jakobs, M. Monkenbusch, D. Richter, T. Sottmann, R. Strey (2000): 'Membrane decoration by amphiphilic block copolymers in bicontinuous microemulsions', *Phys. Rev. Lett.* **85**, pp. 102–105

[22] Endo, H., M. Mihailescu, M. Monkenbusch, J. Allgaier, G. Gompper, D. Richter, B. Jakobs, T. Sottmann, R. Strey, I. Grillo (2001): 'Effect of amphiphilic block copolymers on the structure and phase behavior of oil-water-surfactant mixtures', *J. Chem. Phys.* **115**, pp. 580–600

[23] Fischer, W., E. Koch (1987): 'On 3-periodic minimal surfaces', *Z. Kristallogr.* **179**, pp. 31–52

[24] Fischer, W., E. Koch (1996): 'Spanning minimal surfaces', *Phil. Trans. R. Soc. Lond. A* **354**, pp. 2105–2142

[25] Fodgen, A., S. T. Hyde (1992): 'Parametrization of triply periodic minimal surfaces. I. Mathematical basis of the construction algorithm for the regular class', *Acta Cryst. A* **48**, pp. 442–451

[26] Fodgen, A., S. T. Hyde (1999): 'Continuous transformations of cubic minimal surfaces', *Eur. Phys. J. B* **7**, pp. 91–104

[27] Fontell, K. (1990): 'Cubic phases in surfactant and surfactant-like lipid systems', *Colloid Polym. Sci.* **268**, pp. 264–85

[28] Golubović, L. (1994): 'Passages and droplets in lamellar fluid membrane phases', *Phys. Rev. E* **50**, pp. R2419–R2422

[29] Gompper, G., H. Endo, M. Mihailescu, J. Allgaier, M. Monkenbusch, D. Richter, B. Jakobs, T. Sottmann, R. Strey (2001): 'Measuring bending rigidity and spatial renormalization in bicontinuous microemulsions', *Europhys. Lett.* **56**, pp. 683–689

[30] Gompper, G., J. Goos (1994): 'Fluctuating interfaces in microemulsion and sponge phases', *Phys. Rev. E* **50**, pp. 1325–1335

[31] Gompper, G., J. Goos (1995): 'Fluctuations and phase behavior of passages in a stack of fluid membranes', *J. Phys. II France* **5**, pp. 621–634

[32] Gompper, G., M. Kraus (1993): 'Ginzburg-Landau theory of ternary amphiphilic systems II: Monte Carlo Simulations', *Phys. Rev. E* **47**, p. 4301

[33] Gompper, G., D. M. Kroll (1996): 'Random surface discretizations and the renormalization of the bending rigidity', *J. Phys. I France* **6**, pp. 1305–1320

[34] Gompper, G., D. M. Kroll (1997): 'Fluctuations of polymerized, fluid and hexatic membranes: continuum models and simulations', *Curr. Opin. Colloid Interface Sci.* **2**, pp. 373–381

[35] Gompper, G., D. M. Kroll (1997): 'Network models of fluid, hexatic and polymerized membranes', *J. Phys. Condens. Matter* **9**, pp. 8795–8834

[36] Gompper, G., D. M. Kroll (1998): 'Membranes with fluctuating topology: Monte Carlo simulations', *Phys. Rev. Lett.* **81**, pp. 2284–2287

[37] Gompper, G., D. M. Kroll (2000): 'Statistical mechanics of membranes: Freezing, undulations, and topology fluctuations', *J. Phys. Condens. Matter* **12**, pp. 29–37

[38] Gompper, G., D. Richter, R. Strey (2001): 'Amphiphilic block copolymers in oil-water-surfactant mixtures: Efficiency boosting, structure, phase behavior, and mechanism', *J. Phys. Condens. Matter* **13**, pp. 9055–9074

[39] Gompper, G., M. Schick (1990): 'Correlation between structural and interfacial properties of amphiphilic systems', *Phys. Rev. Lett.* **65**, pp. 1116–1119

[40] Gompper, G., M. Schick (1994): 'Self-assembling amphiphilic systems', in Domb, C., J. L. Lebowitz, eds., 'Phase transitions and critical phenomena', volume 16 (Academic Press, London), pp. 1–176

[41] Gompper, G., S. Zschocke (1992): 'Ginzburg-Landau theory of oil-water-surfactant mixtures', *Phys. Rev. A* **46**, pp. 4836–4851

[42] Góźdź, W., R. Hołyst (1996): 'High genus periodic gyroid surfaces of nonpositive Gaussian curvature', *Phys. Rev. Lett.* **76**, pp. 2726–2729

[43] Góźdź, W., R. Hołyst (1996): 'Triply periodic surfaces and multiply continuous structures from the Landau model of microemulsions', *Phys. Rev. E* **54**, pp. 5012–5027

[44] Große-Brauckmann, K. (1997): 'On gyroid interfaces', *J. Colloid Interface Sci.* **187**, pp. 418–428

[45] Hajduk, D. A., P. E. Harper, S. M. Gruner, C. C. Honeker, G. Kim, E. L. Thomas, L. J. Fetters (1994): 'The gyroid: a new equilibrium morphology in weakly segregated diblock copolymers', *Macromolecules* **27**, pp. 4063–4075

[46] Hajduk, D. A., P. E. Harper, S. M. Gruner, C. C. Honeker, E. L. Thomas, L. J. Fetters (1995): 'A reevaluation of bicontinuous cubic phases in starblock copolymers', *Macromolecules* **28**, pp. 2570–2573

[47] Helfrich, W. (1973): 'Elastic properties of lipid bilayers: theory and possible experiments', *Z. Naturforsch. C* **28**, pp. 693–703

[48] Helfrich, W. (1981): 'Amphiphilic mesophases made of defects', in Balian, R., M. Kleman, J.-P. Poirier, eds., 'Physics of Defects', Les Houches Summer School 1980 (North Holland, Amsterdam)

[49] Helfrich, W. (1985): 'Effect of thermal undulations on the rigidity of fluid membranes and interfaces', *J. Phys. France* **46**, pp. 1263–1268

[50] Helfrich, W., H. Rennschuh (1990): 'Landau theory of the lamellar-to-cubic phase transition', *J. Phys. (Paris) Colloq.* **51**, pp. 189–195

[51] Hildebrandt, S., A. Tromba (1996): *Kugel, Kreis und Seifenblasen. Optimale Formen in Geometrie und Natur* (Birkhäuser Verlag, Basel)

[52] Jahn, W., R. Strey (1988): 'Microstructure of microemulsions by freeze fracture microscopy', *J. Phys. Chem.* **92**, p. 2294

[53] Jakobs, B., T. Sottmann, R. Strey, J. Allgaier, L. Willner, D. Richter (1999): 'Amphiphilic block copolymers as efficiency boosters for microemulsions', *Langmuir* **15**, pp. 6707–6711

[54] Jost, J. (1994): *Differentialgeometrie und Minimalflächen* (Springer-Verlag, Berlin)

[55] Karcher, H. (1989): 'The triply periodic minimal surfaces of Alan Schoen and their constant mean curvature companions', *Manuscripta Math.* **64**, pp. 291–357

[56] Karcher, H., K. Polthier (1996): 'Construction of triply periodic minimal surfaces', *Phil. Trans. R. Soc. Lond. A* **354**, pp. 2077–2104

[57] Koch, E., W. Fischer (1988): 'On 3-periodic minimal surfaces with noncubic symmetry', *Z. Kristallogr.* **183**, pp. 129–152

[58] Kresge, C. T., M. E. Leonowicz, W. J. Roth, J. C. Vartulli, J. S. Beck (1992): 'Ordered mesoporous molecular sieves synthesized by a liquid-crystal template mechanism', *Nature* **359**, pp. 710–712

[59] Kunieda, H., K. J. Shinoda (1982): 'Phase behavior in systems of nonionic surfactant/water/oil around the hydrophile-lipophile-balance-temperature (HLB-temperature)', *J. Dispersion Sci. Technol.* **3**, p. 233

[60] Landau, L. D., E. M. Lifshitz (1970): *Theory of elasticity*, volume 7 of *Course of Theoretical Physics* (Pergamon Press, Oxford), 2nd edition

[61] Landh, T. (1995): 'From entangled membranes to eclectic morphologies: cubic membranes as subcellular space organizers', *FEBS Letters* **369**, pp. 13–17

[62] Lidin, S., S. T. Hyde, B. W. Ninham (1990): 'Exact construction of periodic minimal surfaces: the I-WP surface and its isometries', *J. Phys. France* **51**, pp. 801–813

[63] Lipowsky, R. (1991): 'The conformation of membranes', *Nature* **349**, pp. 475–481

[64] Lipowsky, R., E. Sackmann (1995): *Structure and Dynamics of Membranes*, volume 1A and 1B of *Handbook of biological physics* (Elsevier, Amsterdam)

[65] Longley, W., T. J. McIntosh (1983): 'A bicontinuous tetrahedral structure in a liquid-crystalline lipid', *Nature* **303**, pp. 612–614

[66] Luecke, H., H.-T. Richter, J. K. Lanyi (1998): 'Proton transfer pathways in bacteriorhodopsin at 2.3 **r**Angstrom resolution', *J. Struct. Biol.* **121**, pp. 82–91

[67] Luzzati, V., P. A. Spegt (1967): 'Polymorphism of lipids', *Nature* **215**, pp. 701–704

[68] Luzzati, V., R. Vargas, P. Mariani, A. Gulik, H. Delacroix (1993): 'Cubic phases of lipid-containing systems', *J. Mol. Biol.* **229**, pp. 540–551

[69] Mackay, A. L., H. Terrones (1991): 'Diamond from graphite', *Nature* **352**, p. 762

[70] Mann, S., G. A. Ozin (1996): 'Synthesis of inorganic materials with complex form', *Nature* **382**, pp. 313–318

[71] Matsen, M. W., F. S. Bates (1996): 'Unifying weak- and strong-segregation block copolymer theories', *Macromolecules* **29**, pp. 1091–1098

[72] Mitchell, D. J., G. J. T. Tiddy, L. Waring, T. Bostock, M. P. McDonald (1983): 'Phase behavior of polyoxyethylene surfactants with water', *J. Chem. Soc. Faraday Trans.* **79**, pp. 975–1000

[73] Morse, D. C. (1994): 'Topological instabilities and phase behavior of fluid membranes', *Phys. Rev. E* **50**, pp. R2423–R2426

[74] Morse, D. C. (1997): 'Entropy and fluctuations of monolayers, membranes, and microemulsions', *Curr. Opin. Coll. Interface Sci.* **2**, pp. 365–372

[75] Nelson, D., T. Piran, S. Weinberg, eds. (1989): *Statistical Mechanics of Membranes and Surfaces* (World Scientific, Singapore)

[76] Olsson, U., U. Würz, R. Strey (1993): 'Cylinders and bilayers in a ternary nonionic surfactant system', *J. Phys. Chem.* **97**, pp. 4535–4539

[77] Pebay-Peyroula, E., G. Rummel, J. P. Rosenbusch, E. M. Landau (1997): 'X-ray structure of bacteriorhodopsin at 2.5 **r**Angstroms from the microcrystals grown in lipidic cubic phases', *Science* **277**, pp. 1676–1681

[78] Peliti, L. (1996): 'Amphiphilic membranes', in David, F., P. Ginsparg, J. Zinn-Justin, eds., 'Fluctuating Geometries in Statistical Mechanics and Field Theory', (North-Holland, Amsterdam), pp. 195–285

[79] Peliti, L., S. Leibler (1985): 'Effects of thermal fluctuations on systems with small surface tension', *Phys. Rev. Lett.* **54**, pp. 1690–1693

[80] Pieranski, P., P. Sotta, D. Rohe, M. Imperor-Clerc (2000): 'Devil's staircase-type faceting of a cubic lyotropic liquid crystal', *Phys. Rev. Lett.* **84**, pp. 2409–2412

[81] Pieruschka, P., S. Marčelja (1992): 'Statistical mechanics of random bicontinuous phases', *J. Phys. II France* **2**, p. 235

[82] Pieruschka, P., S. A. Safran (1993): 'Random interfaces and the physics of microemulsions', *Europhys. Lett.* **22**, p. 625

[83] Pieruschka, P., S. A. Safran (1995): 'Random interface model for sponge phases', *Europhys. Lett.* **31**, p. 207

[84] Porod, G. (1951): 'Die Röntgenkleinwinkelstreuung von dichtgepackten kolloiden Systemen 1', *Kolloid Z. Z. Polym.* **124**, p. 83–114

[85] Porte, G. (1992): 'Lamellar phases and disordered phases of fluid bilayer membranes', *J. Phys.: Condens. Matter* **4**, pp. 8649–8670

[86] Porte, G., J. Appell, J. Marignan (1997): 'Comment on "light scattering from the L_3 (sponge) phase: Evidence against logarithmic corrections to ideal scaling"', *Phys. Rev. E* **56**, pp. 1276–1277

[87] Porte, G., M. Delsanti, I. Billard, M. Skouri, J. Appell, J. Marignan, F. Debeauvais (1991): 'Scaling laws for some physical properties of the L_3 (sponge) phase', *J. Phys. II France* **1**, p. 1101

[88] Qiu, H., M. Caffrey (2000): 'The phase diagram of the monoolein/water system: metastability and equilibrium aspects', *Biomaterials* **21**, pp. 223–234

[89] Roux, D., M. E. Cates, U. Olsson, R. C. Ball, F. Nallet, A. M. Bellocq (1990): 'Light scattering from a surfactant 'sponge' phase: Evidence for a hidden symmetry', *Europhys. Lett.* **11**, p. 229

[90] Roux, D., C. Coulon, M. E. Cates (1992): 'Sponge phases in surfactant solutions', *J. Phys. Chem.* **96**, p. 4174

[91] Roux, D., F. Nallet, C. Coulon, M. E. Cates (1996): 'Comment on "thermodynamics of the L_3 (sponge) phase in the flexible surface model"', *J. Phys. II France* **6**, pp. 91–93

[92] Safran, S. A. (1999): 'Curvature elasticity of thin films', *Adv. Phys.* **48**, pp. 395–448

[93] Safran, S. A., D. Roux, M. E. Cates, D. Andelman (1986): 'Origin of middle-phase microemulsions', *Phys. Rev. Lett.* **57**, p. 491

[94] Safran, S. A., L. A. Turkevich (1983): 'Phase diagrams for microemulsions', *Phys. Rev. Lett.* **50**, pp. 1930–1933

[95] Safran, S. A., L. A. Turkevich, P. Pincus (1984): 'Cylindrical microemulsion: a polymer-like phase?', *J. Physique - LETTRES* **45**, pp. L69–L74

[96] Schoen, A. H. (1970): 'Minimal surfaces', NASA Technical Note D-5541, Washington, D.C.

[97] Schwarz, U. S., G. Gompper (1999): 'A systematic approach to bicontinuous cubic phases in ternary amphiphilic systems', *Phys. Rev. E* **59**, pp. 5528 – 5541

[98] Schwarz, U. S., G. Gompper (2000): 'Stability of bicontinuous cubic phases in ternary amphiphilic systems', *J. Chem. Phys.* **112**, pp. 3792 – 3802

[99] Schwarz, U. S., G. Gompper (2000): 'Stability of inverse bicontinuous cubic phases in lipid-water mixtures', *Phys. Rev. Lett.* **85**, pp. 1472–1475

[100] Schwarz, U. S., G. Gompper (2001): 'Bending frustration of lipid-water mesophases based on cubic minimal surfaces', *Langmuir* **17**, pp. 2084–2096

[101] Schwarz, U. S., K. Swamy, G. Gompper (1996): 'The lamellar-to-isotropic transition in ternary amphiphilic systems', *Europhys. Lett.* **36**, pp. 117–122

[102] Scriven, L. E. (1976): 'Equilibrium bicontinuous structure', *Nature* **263**, pp. 123–125

[103] Seddon, J. M., R. H. Templer (1995): 'Polymorphism of lipid-water systems', in Lipowsky, R., E. Sackmann, eds., 'Structure and dynamics of membranes - from cells to vesicles', volume 1A of *Handbook of biological physics* (Elsevier, Amsterdam), pp. 97–160

[104] Seifert, U. (1997): 'Configurations of fluid membranes and vesicles', *Adv. Phys.* **46**, pp. 13–137

[105] Senechal, M. (1990): *Crystalline symmetries - an informal mathematical introduction* (Adam Hilger, Bristol)

[106] Shmueli, U., ed. (1996): *International tables for crystallography. Volume B: Reciprocal space* (Kluwer Academic Publishers, Dordrecht)

[107] Strey, R., W. Jahn, M. Skouri, G. Porte, J. Marignan, U. Olsson (1992): 'Fluid membranes in the water/NaCl-AOT system: A study combining small-angle neutron scattering, electron microscopy and NMR self-diffusion', in Chen, S.-H., J. S. Huang, P. Tartaglia, eds., 'Structure and Dynamics of Strongly Interacting Colloids and Supramolecular Aggregates in Solution', (Kluwer, Dordrecht), pp. 351–363

[108] Strey, R., R. Schomäcker, D. Roux, F. Nallet, U. Olsson (1990): 'Dilute lamellar and L_3 phases in the binary water - $C_{12}E_5$ system', *J. Chem. Soc. Faraday Trans.* **86**, pp. 2253–2261

[109] Strey, R., R. Schomäcker, D. Roux, F. Nallet, U. Olsson (1990): 'On the dilute lamellar and L_3 phases in the binary water-$C_{12}E_5$ system', *J. Chem. Soc. Faraday Trans.* **86**, p. 2253

[110] Templer, R. H., J. M. Seddon, N. A. Warrender, A. Syrykh, Z. Huang, R. Winter, J. Erbes (1998): 'Inverse bicontinuous cubic phases in 2:1 fatty acid/phosphatidylcholine mixtures. the effect of chain length, hydration, and temperature', *J. Phys. Chem. B* **102**, pp. 7251–7261

[111] Teubner, M. (1990): 'Scattering from two-phase random media', *J. Chem. Phys.* **92**, p. 4501

[112] Teubner, M. (1991): 'Level surfaces of Gaussian random fields and microemulsions', *Europhys. Lett.* **14**, p. 403

[113] Teubner, M., R. Strey (1987): 'Origin of the scattering peak in microemulsions', *J. Chem. Phys.* **87**, p. 3195

[114] Thomas, E. L., D. B. Alward, D. J. Kinning, D. C. Martin, D. L. Handlin, L. J. Fetters (1986): 'Ordered bicontinuous double-diamond structure of star block copolymers - a new equilibrium microdomain morphology', *Macromolecules* **19**, pp. 2197–2202

[115] von Schnering, H. G., R. Nesper (1991): 'Nodal surfaces of Fourier series: fundamental invariants of structured matter', *Z. Phys. B* **83**, pp. 407–412

[116] Wang, Z.-G., S. A. Safran (1990): 'Curvature elasticity of ordered bicontinuous structures', *Europhys. Lett.* **11**, pp. 425–430